Data acquisition and signal processing/analysis of scintillation events for the Olympus propagation experiment

Research Report
ISSN 0167-9708
Coden: TEUEDE

Eindhoven
University of Technology
Netherlands

Faculty of Electrical Engineering

Data Acquisition and Signal Processing/Analysis of Scintillation Events for the Olympus Propagation Experiment

by
A.D. Sarma and M.H.A.J. Herben

EUT Report 89-E-232
ISBN 90-6144-232-X

December 1989

Eindhoven University of Technology Research Reports

EINDHOVEN UNIVERSITY OF TECHNOLOGY

Faculty of Electrical Engineering
Eindhoven The Netherlands

ISSN 0167- 9708

Coden: TEUEDE

DATA ACQUISITION AND SIGNAL PROCESSING/ANALYSIS OF SCINTILLATION EVENTS FOR THE OLYMPUS PROPAGATION EXPERIMENT

by

A.D. Sarma

and

M.H.A.J. Herben

EUT Report 89-E-232

ISBN 90-6144-232-X

Eindhoven

December 1989

CIP-GEGEVENS KONINKLIJKE BIBLIOTHEEK, DEN HAAG

Sarma, A.D.

Data acquisition and signal processing/analysis of scintillation events
for the Olympus propagation experiment / by A.D. Sarma and M.H.A.J. Herben. -
Eindhoven: Eindhoven University of Technology, Faculty of Electrical
Engineering. - Fig. - (EUT report, ISSN 0167-9708; 89-E-232)
Met lit. opg., reg.
ISBN 90-6144-232-X
SISO 376 UDC 621.396.946 NUGI 832
Trefw.:elektromagnetische golfvoortplanting; scintillatie / satellietcommunicatie.

Summary

This report starts with the principles of data acquisition of scintillation events to be gathered during the Olympus propagation experiment. After a summary of the errors associated with digital sampling and a review of the scintillation theory, suitable bandwidths are selected for two different experimental set-ups. The procedure to decide the characteristics of the baseband filters , from the basic theory of amplitude and phase scintillation variance and spectral density function, is described, considering different types of analogue and digital filters. A logic circuit to start the sampling of the signals automatically, when the scintillation intensity exceeds a specified level, is also presented. Development of an atmospheric turbulence probe measuring wet and dry bulb temperature fluctuations to support the radio-wave measurements is described, as are details about computer programs for scintillation data analysis. Finally, the realised experimental set-ups are tested using the 11.45 GHz beacon signal of the European Communication Satellite and the signals from the atmospheric turbulence probe.

Sarma, A.D.* and M.H.A.J. Herben§
DATA ACQUISITION AND SIGNAL PROCESSING/ANALYSIS OF SCINTILLATION EVENTS FOR THE OLYMPUS PROPAGATION EXPERIMENT.
Faculty of Electrical Engineering, Eindhoven University of Technology, The Netherlands, 1989.
EUT Report 89-E-232

* Presently with the Wave Propagation Laboratory of the Environmental Research Laboratories, National Oceanic and Atmospheric Administration, 325 Broadway, Boulder, Colorado 80303, U.S.A.

§ With the Telecommunications Division of the Faculty of Electrical Engineering, Eindhoven University of Technology, P.O. Box 513, 5600 MB Eindhoven, The Netherlands

Correspondence concerning this reports should be addressed to the second author.

Contents Page

Acknowledgements

The first author wishes to thank the Olympus Propagation Experiment (OPEX) project leader Mr. J. Dijk for the opportunity to perform the work described in this report. It is a pleasure to thank all the OPEX project staff at EUT for their cooperation.

Sincere thanks are due to the editorial staff at the Wave Propagation Laboratory (ERL, Boulder, USA) for editing and to Mrs. T.J.F.M. Pellegrino (EUT, The Netherlands) for typing the manuscript.

1. INTRODUCTION

Electromagnetic (EM) waves propagating through the atmosphere may undergo random amplitude and phase fluctuations due to random fluctuations in the refractive index of the turbulent troposphere. The measurement of these amplitude and phase scintillations is important for both telecommunication and meteorological research. The importance and effect of turbulence–induced scintillations on radio communication links and on the design aspects of reliable radio communication systems have been studied both theoretically and experimentally by various authors (Gurvich, 1968; Vilar and Haddon, 1984; Medeiros Filho et al., 1983b; Herben and Kohsiek, 1984; Sarma et al., 1986).

Many papers were published on the theory of scintillations. However, less information is available on the practical aspects of data acquisition and signal processing techniques relevant to scintillation measurements (Moulsley et al., 1985; Ortgies, 1985). The present report especially deals with the important points that are to be considered for the data acquisition and processing of scintillation events.

The report is divided into three chapters, besides introduction and conclusions. The second chapter is about the principles of data acquisition of scintillation events to be gathered during the Olympus propagation experiment. After a summary of the errors associated with digital sampling and a review of the scintillation theory, suitable bandwidths are selected for two different experimental set–ups. The procedure to decide the characteristics of the baseband filters, from the basic theory of amplitude and phase scintillation variance and spectral density function, is described, considering different types of analog and digital filters. In chapter three, a logic circuit is presented to start the sampling of the signals automatically, when the scintillation intensity exceeds a specified level. To support the radio–wave measurements, an atmospheric turbulence probe, measuring wet and dry bulb temperature fluctuations, was

developed; this probe is also described in this chapter together with scintillation data analysis. The realised experimental set–ups were tested using the 11.45 GHz beacon signal of the European Communication Satellite and the signals from the atmospheric turbulence probe; the results of these tests are summarised in chapter four.

Even though this report has been written with the objectives of the "Olympus Propagation Experiment (OPEX)" in mind (Barton, 1985), the essence of this report is more or less equally applicable to other measurements such as meteorological data collection in turbulence studies, and optical propagation experiments. Olympus–1 is an experimental three–axis stabilised satellite, designed to meet the payload requirements of future communication satellites and sponsored by the European Space Agency. The satellite will carry a "12.5/20/30 GHz propagation package" besides three other payloads for different purposes. Olympus–1 is designed for a mission lifetime of 7 years and is expected to be operational in 1989. The major aim of OPEX is to collect accurate data on slant path propagation properties of the atmosphere near 12.5, 20 and 30 GHz throughout Europe. Such data are required for the development of propagation prediction models, which are of prime importance in the design of satellite communication systems.

2. THE PRINCIPLES OF DATA ACQUISITION OF SCINTILLATION EVENTS

2.1. Introduction

This chapter consists of 5 sections and completely explains the relevant precautions to be taken for data acquisition of scintillation events. In section two, errors associated with digital sampling are described. The theoretical expressions with respect to the scintillation measurements are presented in section three. Section four is alotted for describing the significance of the scintillation bandwidth selection. The importance of the use of analogue filters is discussed in section five, along with the advantages of digital filters when high sampling rates are used.

The simplified set–up of the scintillation measuring system is shown in Fig. 2.1. The inputs to the analogue to digital converter (ADC) are low–pass filtered baseband signals, representing the amplitude and phase of the EM waves and meteorological signals such as temperature and humidity. The pre–processing of the digital data includes digital filtering, if necessary. The resulting pre–processed digital data are used for spectral analysis, variance estimation, and probability distribution estimation.

2.2. Errors associated with digital sampling

The conversion of continuous signal information into sampled digitally coded form is necessary for signal processing. The following errors can be associated with the sampling of a continuous signal. Most of these errors are discussed in detail elsewhere (Bendat and Piersol, 1971; Shanmugam, 1979; Brigham, 1974).

– Quantisation error

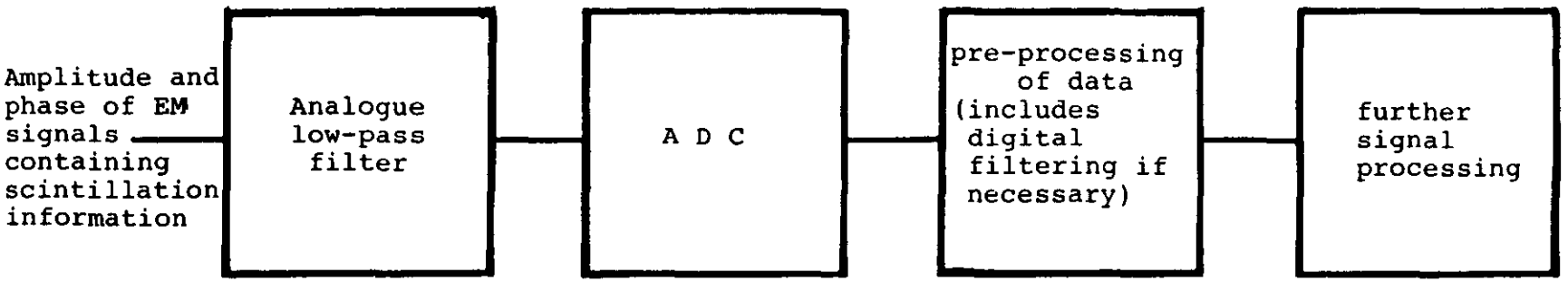

Figure 2.1 Simplified set-up of the scintillation measuring system.

The whole input range of the ADC is divided into a fixed number of quantisation levels. The quantisation error equals the quotient of the input range and the number of quantisation levels. For example, a 12–bit ADC, with 4096 quantisation levels has a quantisation error of 1.22 mV for an input range of 10 V.

– Leakage

Any practical measurement of the power spectral density from a finite record of data samples may only be considered as an estimate ($\bar{G}(f)$), having an error relationship to the true value (G(f)). This is because the raw power spectral density function is the result of the convolution of the true power spectral density function with the Fourier transform of the window function used. This effect causes leakage by spreading the main lobe of G(f) and by adding an infinite number of smaller sidelobes because of the truncation. Leakage reduces the accuracy of $\bar{G}(f)$. The leakage can be reduced by employing a time domain truncation function, different from the rectangular one, which has a sidelobe envelope below that of the sinc function.

– Aperture error

The data sample is taken over a finite period of time rather than instantaneously, causing aperture error.

– Jitter

Sometimes the time interval between samples can vary slightly in some random manner, causing jitter.

– Nonlinearities

Uneven spacing between quantisation levels and variation of gain with frequency of a tape recorder on which the analogue signals are stored etc., are the sources of these

errors.

– Aliasing error

This is one of the most important errors associated with analogue–to–digital conversion, which can be reduced but never totally eliminated. The sampling theorem states that at least two samples per cycle are required to define a frequency component in the original data. So the Nyquist frequency (f_c) of a continuous random signal sampled at a time interval Δt is equal to $1/2\Delta t$. Sampling with a smaller time interval will lead to confusion between the low and high frequency components of the original data. This problem is known as aliasing. For any frequency f in the range $0 \leq f \leq f_c$ the higher frequencies which are aliased with f are given by $(2 f_c \pm f)$, $(4f_c \pm f)$ ..... $(2n f_c \pm f)$. The usual practical way to reduce aliasing errors in digital data analysis is to remove that information in the analogue signal that might exist at frequencies above f_c prior to the A/D conversion, by restricting the frequency range of the original signal with an analogue low–pass filter prior to ADC. Such filters are commonly known as anti–aliasing filters.

2.3 Theoretical background of tropospheric scintillations

The most important aims of scintillation measurements are the estimation of the scintillation variance and the spectral density function. Frequencies in the window region and absorption region were dealt with by various authors, both theoretically (Tatarskii, 1961; Ishimaru, 1978; Ott and Thompson, 1978) and experimentally (Vilar and Haddon, 1984; Medeiros Filho et al., 1983; Herben and Kohsiek, 1984; Sarma et al., 1986). Their results are useful when choosing the filter characteristics for the scintillation measurements.

The expression for the log–amplitude fluctuations is written as

$$\chi \triangleq \ln \left(\frac{A}{A_0}\right) \tag{2.1}$$

where A is the amplitude of the received wave and A_0 is the amplitude of the wave at the receiver in the absence of tropospheric turbulence. In practice, it is impossible to measure the value of A_0; hence A_0 can be taken as the time–average value of A ($A_0 = \langle A \rangle$). The intensity of the amplitude fluctuations in decibels is defined as

$$I_{dB} \triangleq 20 \log \left(\frac{A}{\langle A \rangle}\right). \tag{2.2}$$

Using these definitions, expressions are presented for the variance and spectrum of the log–amplitude and phase scintillations. All the following equations were derived assuming a point receiver and are meant for the plane wave case, which holds for satellite–to–earth propagation paths. In case of a non–point receiver, the width of the scintillation spectrum decreases as the effective aperture radius of the antenna increases. The complete analysis of this effect is treated by van Weert (1975). So the bandwidth of the baseband filter obtained from the following equations is sufficiently large for the non–point receiver case also.

2.3.1 The operating frequency is in the window region

The variance of the log–amplitude fluctuations due to turbulent scattering can be written as (Tatarskii, 1961)

$$\sigma_\chi^2 = 0.31\, C_{nR}^2\, k^{7/6}\, L^{11/6} \tag{2.3}$$

where χ is the logarithm of the ratio between fluctuating and average amplitudes (2.1). C_{nR}^2 is the average real refractive index structure parameter obtained by integration

over the effective atmospheric propagation path with length L, and k (= 2 π/λ) is the wave number.

The asymptotic forms of the temporal scintillation power spectral density function in the low ($\frac{\omega}{v}\sqrt{\frac{L}{k}} < 1$) and high ($\frac{\omega}{v}\sqrt{\frac{L}{k}} > 1$) frequency regions can be written as (Medeiros Filho et al., 1983b)

$$W_{\chi}^{o}(\omega) = 0.85\, C_{nR}^{2}\, \frac{L}{v}\, k^{2}\, (\frac{L}{k})^{4/3} \tag{2.4}$$

$$W_{\chi}^{\infty}(\omega) = 2.19\, C_{nR}^{2}\, \frac{L}{v}\, k^{2}\, (\frac{\omega}{v})^{-8/3} \tag{2.5}$$

respectively, where v is the average wind speed transverse to the propagation path and ω is 2π times the scintillation frequency.

These two asymptotes to the spectral density meet at a frequency f_{c2} given by

$$f_{c2} = 0.57\, \frac{v}{\sqrt{\lambda L}} \quad \text{Hz.} \tag{2.6}$$

The asymptotic forms of the phase spectra $W_{\varphi}(\omega)$ in the low ($\frac{\omega}{v}\sqrt{\frac{L}{k}} < 1$) and high ($\frac{\omega}{v}\sqrt{\frac{L}{k}} > 1$) frequency regions can be related to the asymptotic form of the amplitude spectrum in the high frequency region as (Ishimaru, 1978)

$$W_{\varphi}^{o}(\omega) \to 2W_{\chi}^{\infty}(\omega) \quad \text{for } \omega \to 0 \tag{2.7}$$

$$W_{\varphi}^{\infty}(\omega) \to W_{\chi}^{\infty}(\omega) \quad \text{for } \omega \to \infty \tag{2.8}$$

Examples of temporal frequency spectra of the log–amplitude fluctuations $W_{\chi}(\omega)$ and the phase fluctuations $W_{\varphi}(\omega)$ normalised to $W_{\chi}(0)$ are shown in Fig. 2.2.

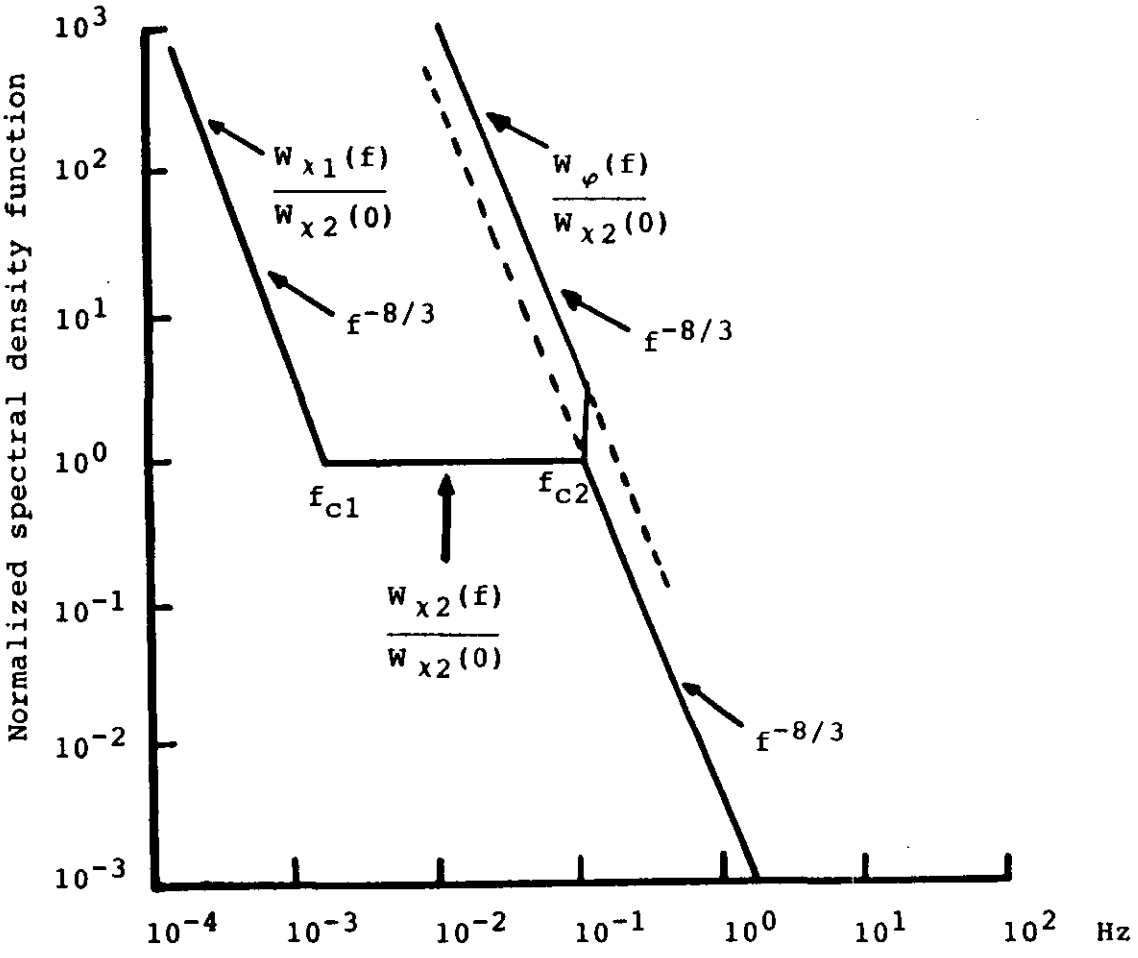

Figure 2.2 Temporal frequency spectra of the log-amplitude fluctuations $W_{x1,2}(f)$ and phase fluctuations $W_{\varphi}(f)$ normalized to $W_{x2}(0)$. W_{x1}: Operating frequency in the absorption region. W_{x2}: Operating frequency in the window region.

Finally, the two asymptotic expressions to the spectral density function of the differential phase scintillations of two coherent signals (k_1, k_2; $k_1 < k_2$) in the low ($\frac{\omega}{v}\sqrt{\frac{L}{k_1}} < 1$) and high ($\frac{\omega}{v}\sqrt{\frac{L}{k_1}} > 1$) frequency regions can be written as (Sarma et al., 1986)

$$W^{o}_{\varphi d}(\omega,k_1,k_2) = 4.38\, C^2_{nR}(k_1-k_2)^2\, \frac{L}{v}\, (\frac{\omega}{v})^{-8/3} \tag{2.9}$$

$$W^{\infty}_{\varphi d}(\omega,k_1,k_2) = 2.19\, C^2_{nR}(k_1^2+k_2^2)\, \frac{L}{v}\, (\frac{\omega}{v})^{-8/3} \tag{2.10}$$

respectively. Hence, the asymptotes to the high and low frequency ends of the differential phase spectrum will be expected to show a –8/3 slope with a ratio between them of $(k_1^2+k_2^2)/2(k_1-k_2)^2$. The general shape of the theoretical differential phase spectrum is shown in Fig. 2.3.

2.3.2 The operating frequency is in the absorption region

The variance of the log–amplitude fluctuations due to turbulence can be written as

$$\sigma^2_{\chi} = 0.31\, k^{7/6}\, L^{11/6}\, (C^2_{nR}I_R - C_{nRI}I_{RI} + C^2_{nI}I_I) \tag{2.11}$$

where C^2_{nR} and C^2_{nI} are the structure parameters of the real and imaginary part of the refractive index and C_{nRI} is the joint structure parameter between the real and imaginary part of the refractive index. The integrals I_R, I_I and I_{RI} are defined elsewhere (Jayasuriya et al., 1981).

The asymptotic form to the amplitude scintillation spectral density function in the low frequency region ($\frac{\omega}{v}\sqrt{\frac{L}{k}} < 1$) is given by (Medeiros Filho et al., 1983b)

$$W^{o}_{\chi}(\omega) = W_{\chi R}[1+5.15 \frac{C^2_{nI}}{C^2_{nR}} (\frac{k}{L})^{4/3} (\frac{\omega}{v})^{-8/3}] \qquad (2.12)$$

with $W_{\chi R} = W^{o}_{\chi}(\omega)$ (Equation 2.4).

The asymptotic form to the spectral density in the high frequency region ($\frac{\omega}{v}\sqrt{\frac{L}{k}} > 1$) is the same as in Equation 2.5.

Unlike the lossless case, this case has two corner frequencies. The lower corner frequency (f_{c1}), defined as the frequency where $W^{o}_{\chi}(\omega)=2W_{\chi R}(\omega)$, is given by

$$f_{c1} = 0.74 [\frac{C^2_{nI}}{C^2_{nR}}]^{3/8} \frac{v}{\sqrt{\lambda L}} \text{ Hz.} \qquad (2.13)$$

The expression for upper corner frequency (f_{c2}) is the same as that given by Equation 2.6. The absorption has no effect on either the absolute or differential phase scintillation spectrum and is therefore the same as for the lossless case (2.7–10). More information about the influence of oxygen absorption on frequencies near 60 GHz can be found elsewhere (Sarma, 1988).

Even for the absorption free case, recently it has been reported that (Herben, 1986; Herben, 1983b), on a 8.2 km line–of–sight terrestrial link at 30 GHz, rain induced scintillations can be distributed over a wider scintillation frequency band, with enhancements at both low and high frequency regions, than the turbulence–induced tropospheric scintillations. Similar observations were made on a satellite–earth link at 11 GHz (Ortgies, 1985) and on a line–of–sight link at 230 GHz (Sarma et al., 1990;Hill et al., 1989). In their work Sarma et al. (1990) found two additional corner frequencies at the high frequency end of the scintillation spectrum. The enhancements are due to variable attenuation and incoherent scattering by rain. Therefore, it is necessary to analyse both high and low frequency regions of the scintillation spectrum.

If the scintillation signals are expressed in power decibels, all the amplitude power spectral density functions presented in this section are to be multiplied by 75.4 (Equation 2.2), in order to obtain the results in the units dB^2/Hz, for the phase signals no multiplication is needed to obtain the power spectral density functions in the units rad^2/Hz.

2.4 Bandwidth selection for scintillation measurements

It will be clear from Sec. 2.3 that a large variety of scintillation behaviours of the signals may be observed during propagation experiments. The scintillation frequency range can be divided into the low frequency region and the high frequency region. It is often difficult to give a clear–cut demarcation between these two regions. However, it is convenient to assume the following:

(a) When the operating frequency is in the window region, the amplitude scintillation frequencies lying below the corner frequency f_{c2} (Equation 2.6) are low frequency components, and the frequencies lying above f_{c2} are high frequency components. Experimentally estimated typical values for f_{c2} lie in the range 0.1 to 1 Hz (Vilar and Haddon, 1984; Herben and Khosiek, 1984; Moulsley et al., 1985). The value of f_{c2} is variable and depends on the prevailing wind speed transverse to the propagation path. The observed amplitude and phase fluctuations are due to the variations of the real part of the refractive index (Equation 2.3). This can be understood as the scattering caused by refractive index irregularities in the transparent medium.

(b) When the operating frequency is in the absorption region, the amplitude spectrum (Fig. 2.2) will have a lower corner frequency (f_{c1}) and an upper corner frequency (f_{c2}). The frequencies below f_{c1} are generally termed as low frequency components, whereas the frequencies above f_{c2} are known as high frequency components. Typical experimental values for f_{c1} lie in the range 10^{-3} to 10^{-2} Hz (Medeiros Filho et al.,

1983b). The value of f_{c1} is highly variable and depends on prevailing meteorological conditions as described by equation 2.13 and also on whether the temperature or water vapour pressure fluctuations are predominant (Sarma and Cole, 1987; Cole et al., 1988). The corner frequency f_{c1} increases if the absorption increases. Values of f_{c2} will lie in the same range as in case (a).

It was observed in the case of the line–of–sight terrestrial path that when natural atmospheric turbulence is the main mechanism responsible for the scintillations, the large horizontal scale sizes which can be of the order of hundreds of meters cause enhancement in the low–frequency region of the amplitude spectrum (Jayasuriya et al., 1981). This is in contrast to the usually assumed value of the vertical scale size, which is comparable with the height of the link above the ground level or, in the case of stratified layers, the thickness of the layer. The magnitude of the absorption–induced scintillations, relative to the pure scattering induced scintillations, is related to the refractive index structure parameters and the integrals I_R, I_{RI} and I_I which are a function of the outer scale of turbulence, thus justifying Equation 2.11 for the variance. For scintillation frequencies greater than the corner frequency f_{c2} (Fig. 2.2), the scattering mechanism dominates the absorption mechanism in the amplitude spectrum. For scintillation frequencies smaller than the corner frequency f_{c1} the absorption mechanism dominates the scattering mechanism in the amplitude spectrum. In this low frequency region the signal fluctuations are caused by the variations of the imaginary part of the refractive index, i.e., absorption fluctuations that can be considered to be due to variations in the optical thickness of the medium. At intermediate values of the scintillation frequencies, between f_{c1} and f_{c2}, both scattering and absorption mechanisms are correlated and their effect on the amplitude spectrum is as shown in Fig. 2.2. It is evident that the spectra show a –8/3 slope in both the high frequency and the low frequency regions. Under clear–sky conditions, when the operating frequency is in the window region (and there is no rain), the –8/3 slope in the low frequency region

is absent.

Because all the expressions quoted earlier are asymptotic expressions, it is preferable to have as many frequency points as possible in the spectra to check the validity of the theory and estimate the corner frequencies reliably. However, one cannot choose a detection bandwidth of the scintillation measuring system and a sampling frequency that are arbitrarily large. The limiting factors on the highest frequency in the spectra are the computer's processor speed, which puts an upper limit on the sampling frequency, and the receiver noise, which puts a limit on the phase–locked–loop receiver bandwidth. A phase–locked–loop system which provides signals with a bandwidth of about 50 Hz is acceptable (Barton, 1985). Generally, the scintillation process contains relevant information up to 10–20 Hz. In order to investigate the influence of large outer scale size turbulence on the spectra in the absorption case, the low frequency components are to be estimated experimentally. The effect of the outer scale of turbulence and wavelength on scintillation fading at millimeter wavelengths is treated elsewhere (Cole et al., 1978).

In the lossless case, for clear–sky conditions, the low frequency enhancement is absent. Hence it appears that the low frequency of interest is not critical and is usually about 10^{-2} Hz, which is sufficient for the corner frequency f_{c2} to be detected. For other conditions, the selection of the lowest frequency of interest is more complex.

In choosing the lowest frequency for the OPEX (with all beacons in the window region) the following points are to be noted:

a) It is worth investigating thoroughly whether there is any low frequency enhancement at 20 and 30 GHz under adverse weather conditions.

b) When differential phase measurements are being made of two coherent signals, for instance 20 and 30 GHz beacon signals of Olympus, caution should be exercised because there exists a –8/3 asymptotic slope in the low frequency regions also (see Fig. 2.3). The ratio between the low and high frequency asymptotes depends upon the operating

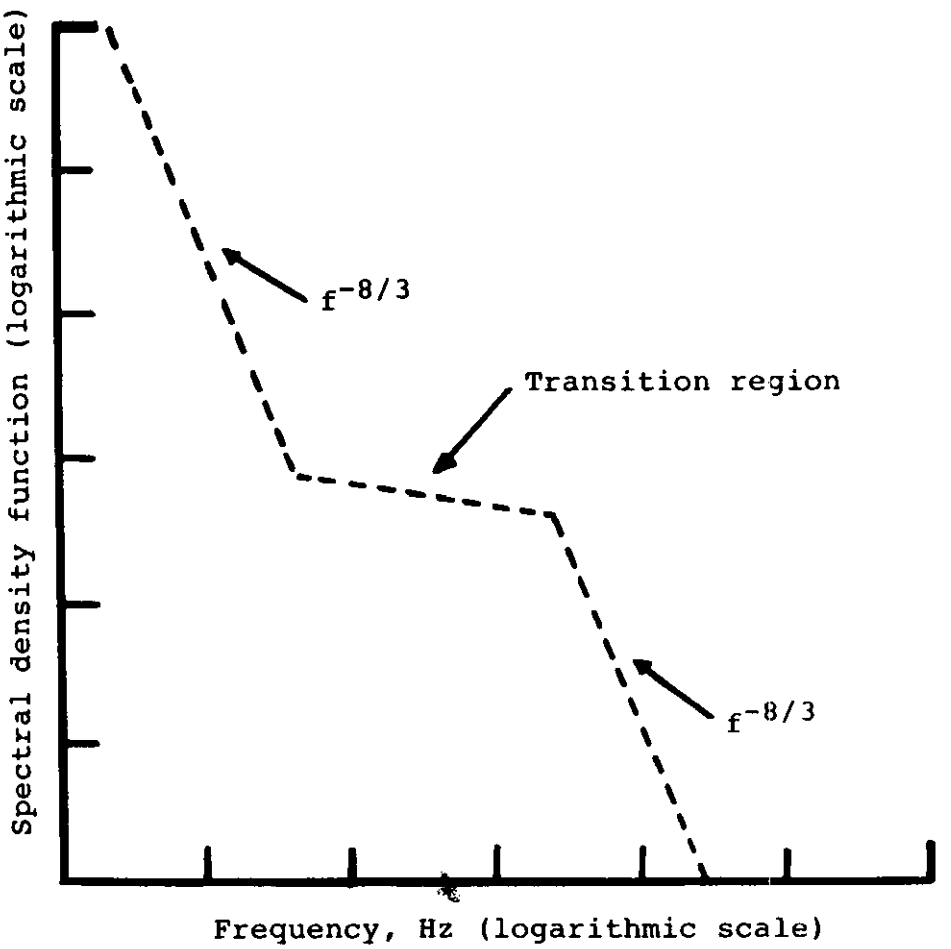

Figure 2.3 General shape of the theoretical differential phase spectrum.

frequencies and the separation between them (Equations 2.9 and 2.10) (Sarma et al., 1986; Sarma and Herben, 1990b). In the case of differential phase spectrum of the 20 and 30 GHz signals the ratio is about 8 dB. The ratio estimated from the experimental spectrum could be used to verify the theoretical model adopted.

Taking these points into consideration for the OPEX, it is reasonable to set up a low frequency limit as low as possible. However, the lowest frequency should not be below approximately 4×10^{-4} Hz for the following reasons:

a) It is usual to obtain a frequency spectrum with a segment consisting of 1024 data samples. Hence, to obtain the lowest frequency of this order the sampling frequency should be about 0.4 Hz. To obtain this data requires 42.6 minutes. To improve statistical reliability it is usual to take two or more such segments. If four such segments are taken, the time required is about 2.8 hours.

b) It is preferable to take scintillation measurements for not more than 3 to 4 hours, since it is then difficult to correlate radio measurements with the meteorological measurements because the assumption that the signals are stationary becomes tenuous.

However, long–term tropospheric scintillation variance statistics can be taken for much longer periods (months or even years) with a limited bandwidth (0.02 to 2.5 Hz) (Moulsley and Vilar, 1982). The lower limit is set to avoid the problems of contaminating the true data by a slowly varying component, which is not related to scintillations but rather is caused by spacecraft effects, attenuation or receiver drifts. However, these spacecraft or other effects, are supposed to be absent for the relatively short term measurements (3 to 4 hours) mentioned earlier. There are two main reasons for selecting the upper limit as 2.5 Hz:

a) Measurements of scintillation power spectra indicate that the scintillation spectrum typically exhibits a corner frequency in the range 0.1 to 1 Hz. Therefore, most of the scintillation power is concentrated at the Fourier components below this frequency.

b) As these statistics are to be accumulated on a long term basis and the processing of

data is expected to be done in real time, one cannot afford to use high sampling rates because of the computer's limited processor speed.

For the following set of typical experimental conditions that are expected to be encountered during OPEX, some of the values related to scintillation data can be estimated as follows. The elevation angle of the ground station antenna is greater than 10 degrees, so multipath effects may be neglected. The effective slant–path length for such an earth–space link (Vilar and Haddon, 1984) (L) = 5.0 km. Assume an average transverse wind speed (v) = 1 m/s. For the operating frequency = 30 GHz, the upper corner frequency f_{c2} can be calculated using Equation 2.6 as 0.08 Hz.

The range of the incoming signal is expected to vary between 0 and 1 dB^2 (Mawira, 1986). With 1 dB^2 variance the frequency independent horizontal portion of the amplitude scintillation spectrum will be 7.7 dB^2/Hz (Equations 2.2–4). Suppose the incoming signal has a Gaussian distribution and 99.8% of the time the signal lies in the region of acceptance. Then the incoming signal power can be considered to be varying between –3.1 dB and +3.1 dB, corresponding to 1 dB^2 variance. Even though it is usual to describe the probability distribution between 5% and 95% of levels, the high percentage of time (99.8%) in the acceptance region is selected to facilitate the reconstruction of the signal spectrum corresponding to the whole frequency region of interest. Moreover, it is reported that the gaseous absorption mechanism causes a significant departure at the extremes of the log–normal distribution usually obtained for frequencies in the atmospheric windows (Medeiros Filho et al., 1983a). Therefore, it is important to take into consideration as much percentage of confidence interval as possible for estimating the distribution of the incoming signal scintillations, in order to investigate any possible effect due to passing clouds, etc..

2.5. Selection of filters

The occurrence of propagation events of interest is infrequent and random in nature. Hence, care must be taken in the acquisition of propagation events data. It is most important in scintillation measurements to eliminate the false data introduced by equipment disturbances, aliasing errors or quantisation errors. Otherwise, the biased data could mask the propagation effects. Some of these errors can be significantly reduced by using appropriate filters. There are many popular filters available. One of the objectives of this report is to present some useful tips in choosing economical and simple filters for scintillation measurements.

As it is necessary to have such a wide scintillation bandwidth (4×10^{-4} to 20 Hz), it is not possible to get all the frequency components with a sufficient statistical reliability by analysing one segment of data points (1024). Therefore, it is the usual practice to divide the scintillation spectrum into two or more frequency regions with sufficient overlap (Medeiros Filho et al., 1983b, Sarma and Herben, 1989). The whole bandwidth of interest can be covered by sampling the signal at 40 Hz; to obtain the lower part of the frequency spectrum, the sampled data can be decimated (Bendat and Piersol, 1971).

In general, when compared to other sources of error, quantisation errors are usually unimportant. However, in the case of scintillation measurements care must be taken that the analogue data occupy as much of the available input range of the ADC as possible. Otherwise, the resolution will be poor and the quantisation error could become significant. For example, if the full range of signal is quantised at 40.96 scale units of a 12–bit ADC instead of 4096, the peak signal to rms noise ratio would be reduced by 40 dB. Therefore, it is preferable to amplify the signals to utilise the full dynamic range of the ADC, after taking into account the maximum expected variance of the signal. In any case, the quantisation noise should be kept below the receiver

noise level, which will put a limit on the minimum detectable scintillation signal.

In order to minimise the aliasing errors, the following points can be taken into account before choosing a filter for the scintillation measurements:

a) Aliasing effects can be minimised by bandlimiting the signal by filtering before sampling.

b) Even an anti–aliasing filter is used before sampling, the frequencies around f_c are unavoidably most affected. However, the effect can be minimised by using a filter with an almost rectangular transfer function. So, a filter with a small ripple in the passband, and a steep slope starting at f_c could be a good choice.

c) Another way to minimise the aliasing error is to sample at a rate moderately higher than the normal Nyquist rate and decimate the sampled data according to the frequency range of interest using an appropriate digital filter. However, when a high sampling rate is used, it is better to have the cut–off frequency of the analogue low–pass filter less than 50 Hz to avoid noise due to hum (supply frequency). Otherwise, a sampling frequency of 60 Hz will result in a 50 Hz hum input that is indistinguishable from a 10 Hz input signal.

The amplitude characteristics of the commonly used filters are dealt by Johnson et al. (1980). It appears that a 6^{th} order Chebyshev filter meets most of the scintillation measurement requirements and hence it is one of the good choices. The Chebyshev filter is sometimes called an equi–ripple filter because it has ripples of equal magnitude in the passband and is monotonic elsewhere. In some applications phase match is important and hence care is to be taken regarding this.

For the case of OPEX, the above discussed errors can be estimated using the typical experimental conditions (given in the previous section) as follows:

Detected voltage signals, corresponding to the EM signals, can be obtained from the receiver either in logarithmic form or linear form. In logarithmic form, equal variations in the detected voltage correspond to equal variations in the signal power in decibels.

In linear form, the detected voltage corresponds to the amplitude variations in voltage. It is assumed here that the detected voltages are available in logarithmic form.

A 30 GHz Olympus beacon receiver, having a 3 m antenna and a detection bandwidth of 50 Hz, is expected to have a signal–to–noise ratio (CNR) of 44.4 dB and a dynamic range of about 40 dB (Barton, 1985). Thermal noise induces two types of errors, namely, bias errors (ΔT_B) and random errors (ΔT_R). These errors limit the accuracy of the system and are defined as (Robins, 1978)

$$\Delta T_B = 10 \log (1 + 1/CNR) \text{ dB} \tag{2.14}$$

$$\Delta T_R = 10 \log (1 + \sqrt{2/CNR}) \text{ dB}. \tag{2.15}$$

ΔT_B can be neglected in the presence of high CNR's. For the present example the random error can be calculated using equation (2.15) as 0.037 dB.

Tropospheric scintillations and receiver equipment disturbances, such as small linear drifts, may cause enhancement in the signal level up to several decibels ($\sim$ 6 dB). Therefore, a total of about 46 dB is to be accommodated in the full dynamic range of the 12–bit ADC. Due to non–linearity, in practice M–bit converters exhibit the quantisation noise of (M–1) bit converters (Travis, 1985). So, the practical resolution of a 12–bit ADC approximates the theoretical resolution of a 11–bit ADC, which is equal to 0.022 dB. As the quantisation noise has a standard deviation of 0.29 scale unit, the noise due to quantisation (σ_q) will be equal to 0.006 dB which is smaller than the error induced by thermal noise. That means, as far as the variance estimation measurements are concerned, the influence of quantisation noise cannot be reduced either by amplifying or oversampling the signal (when $\Delta T_R > \sigma_q$). However, when the data are used for spectral analysis, it is preferable to keep the quantisation spectral density as low as possible in order to investigate the high frequency spectral

components more accurately. Oversampling the signal by a factor of two reduces the spectral density due to quantisation noise to half its value. If the computer speed/memory limits the sampling rate, the scintillation signals can be appropriately amplified. For the 100 Hz sampling rate, the quantisation spectral densitywould be 3.6 x 10^{-7} dB^2/Hz (Shanmugam, 1979), whereas the spectral density due to thermal noise is about 2.7 x 10^{-5} dB^2/Hz. The spectral density due to tropospheric scintillation at a scintillation frequency of 20 Hz can be calculated, in terms of its variance, using Equations (2.2), (2.3) and (2.5) as 2.39 x 10^{-4} σ_χ^2 dB^2/Hz. With the signal variance of 1 dB^2 the value of the power spectral density becomes equal to 3.17 x 10^{-6} dB^2/Hz at a scintillation frequency of 20 Hz. So the spectral density due to thermal noise is about 1 decade above the signal level at 20 Hz scintillation frequency. Therefore, the conclusion for this specific example is that it is not possible to see the scintillation effects around 20 Hz. Obviously, there is no necessity of amplifying the signal to bring down the spectral density due to quantisation noise which is about 2 decades less than that due to thermal noise.

A 6^{th}–order Chebyshev filter, having a ripple of 0.1 dB and a slope of about 46 dB/octave starting at f_c, is chosen as an anti–aliasing filter. The cut–off frequency of the filter is set to 40 Hz to facilitate high sampling rates (100 Hz). Therefore, the error in the frequency range of interest (4 x 10^{-4} – 20 Hz), either due to ripple of the filter or due to the aliasing effect, will be less than or about 0.1 dB, which is sufficient for most of the scintillation measurements.

2.5.1. Filter configuration suitable for adverse weather conditions

For scintillation measurements during adverse weather conditions such as rain, a different type of filtering configuration is to be used if the signals are available in a linear form. This is because, during such conditions, the signal can show attenuations

up to tens of decibels. The relatively small and fast scintillations are superimposed on the large, slowly varying, attenuation components caused by rain. If all these variations are accommodated in the whole range of the ADC, the signal–to–quantisation noise ratio will be very much reduced compared with the previous example, especially at the higher attenuations. Therefore, the filter configuration suggested by Herben (1986) (see Fig. 2.4), for the case of linear signal, may be considered depending on the available CNR. If the linear signal is sampled during rain, the fast and small amplitude scintillations are masked by quantisation noise. In order to avoid problems with the quantisation noise for the small, rapidly varying component (bandpass filtered [BPF] signal) of the co–polar signal, this component is first separated from the larger slowly varying component (low pass filtered [LPF] signal). The ratio of the amplification of the BPF signal and the LPF signal was 64.5 for the propagation experiment described by Herben (1986). So the quantisation noise for the relatively small BPF signal was reduced by 36.2 dB.

In the present discussion it is assumed that the signal is available in logarithmic form. As stated earlier, the influence of thermal noise varies with CNR. For a rain attenuation of 40 dB, the CNR of the 30 GHz beacon reduces to 4.4 dB within the 50 Hz bandwidth and consequently the spectral density due to thermal noise increases to a level of about 0.3 dB^2/Hz (Equations 2.14–2.15). With this value of thermal noise spectral density, the scintillation noise is almost completely masked by the thermal noise. Hence, for this specific example, it is not necessary to use the filter network shown in Fig. 2.4.

2.5.2. Digital filters

As mentioned earlier, it is preferable to select a high sampling rate to minimise the aliasing errors. When a high sampling rate is used the sampled data have to be filtered

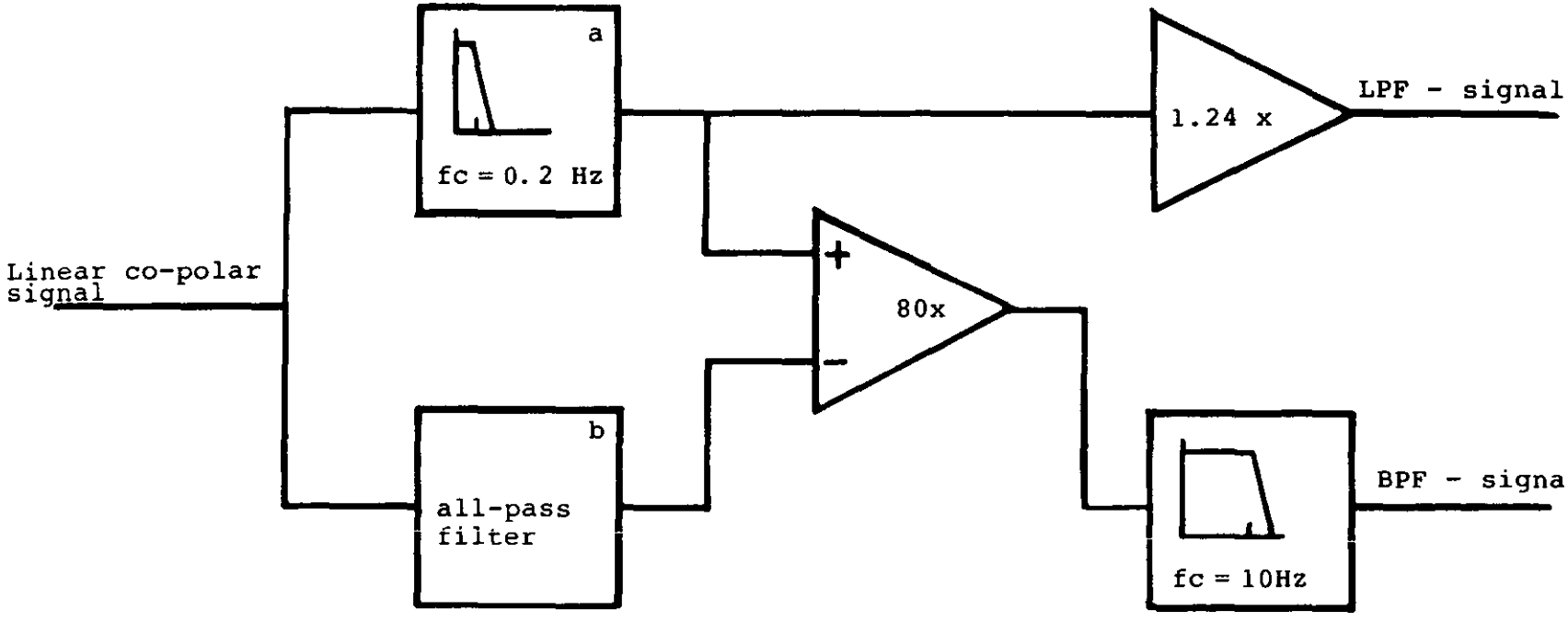

Figure 2.4 Circuit for separating the LPF and BPF signals.
a. 6th order Bessel-filter with 0.2 Hz cut-off frequency.
b. all-pass filter with the same phase characteristic as the Bessel filter (a).
c. 6th order Chebyshev filter with 10 Hz cut-off frequency (anti-aliasing filter).

digitally before decimation in order to extract information in the frequency region of interest. Some of the salient features and relative advantages of digital and analogue filters are listed in Table 2.1.

Digital filters can be divided into two classes, viz., recursive and non–recursive. In contrast to the non–recursive filter, the recursive filter incorporates feedback and has a non–linear phase characteristic. Much information on the design and implementation of digital filters is available (Peled and Liu, 1976; Crochiere and Rabiner, 1981). Here only relevant information is mentioned briefly. The relative aspects of recursive and non–recursive filters are listed in Table 2.2. Even though the phase characteristics of digital filters for most of the scintillation measurements are not critical, in this work a non–recursive digital filter is chosen for use in signal pre–processing.

To achieve a specified frequency response, several design methods are available for the realisation of non–recursive filters and some of them were dealt with sufficient detail by Crochiere and Rabiner (1981).

In the present work the "optimal, equi–ripple linear phase design technique" (Peled and Liu, 1976) is proposed in developing the non–recursive filter. The design is based on the Chebyshev approximation method. The algorithm uses the Remez exchange method in order to design the filter with minimum weighted Chebyshev error in approximating the desired ideal response. The filter response is optimal in the sense that the peak (weighted) approximation error in the frequency domain, over the frequency range of interest, is minimised. It is easy to determine the number of taps in the low–pass filter, to meet any set of design specifications, using the widely available design charts and tables (Crochiere and Rabiner, 1981). Conversion to high/bandpass filter response is simple.

Table 2.1. Relative advantages of analogue and digital filters

Specification	Analogue filter	Digital filter
Accuracy	Difficult to obtain components having tolerances less than 1% and hence difficult to control background noise	The inaccuracies in a digital filter are due to the rounding errors in the computer arithmetic and can be made as small as possible.
Versatility	Relatively difficult to produce complicated filter characteristics, for practical reasons	A computer can be easily programmed to obtain complicated filter characteristics.
Freedom from drift	Characteristics of filters can change due to variations in supply voltages and ambient temperature, etc.	The characteristics of digital filters remain the same.
Nature of input	Generally operates on waveforms	Only operates on sequence of numbers
Operating time	Real time filter	Real time operation is possible, depending on computer's processor speed and sample frequency of the input signal.

Table 2.2. Relative aspects of recursive and non–recursive filters

Description	Comparison
Feedback	Recursive filters incorporate feedback in contrast to non–recursive filters.
Stability	Relatively more care is to be taken in ensuring stability in the case of recursive filters whereas in the case of non–recursive filters, after a particular length of time, the effect of large spurious input such as switching transient disappears completely. Stability is guaranteed under all circumstances.
Simplicity	Compared with non–recursive filters, a given gain characteristic can be obtained with much lower order if a nonrecursive filter is used.
Economy	For a given gain characteristic, recursive filters are more economical in terms of computer memory and time.
Phase characteristic	Recursive filters have the disadvantage of having a non–linear phase characteristic in contrast to non–recursive filters.
Design easiness	Compared with recursive filters, non–recursive filters are easy to design for a given gain characteristic.

3. DATA ACQUISITION SET–UPS AND SIGNAL ANALYSIS

3.1. Introduction

In this chapter three types of experimental set–ups are discussed which can be implemented for different purposes. The first set–up is meant for normal scintillation bandwidth analysis and is expected to be used most of the time. The second is for wide scintillation bandwidth analysis, using variable cut–off frequency filters. The third one is for the acquisition of scintillation events at chosen time intervals, using a logic circuit to start the sampling of the signals automatically.

Twelve signals are identified for data acquisition. Nine of them correspond to the absolute amplitude, differential amplitude and differential phase of the three beacon signals from the Olympus satellite. The remaining three are the dry and wet bulb temperature signals from the atmospheric turbulence probe and the signal from the wind speed meter. Data on wind direction are fed into a separate computer system. Details about the developed tropospheric turbulence probe are also given in this chapter.

Further, the signal processing techniques for scintillation event analysis are described. These include signal preprocessing and storage of the final results. The signal preprocessing includes digital filtering, decimation, linear trend removal and stationarity test operations. In this way the amount of data can be substantially reduced. Actual algorithms and listing of all the computer programs for data acquisition and signal preprocessing can be found elsewhere (Sarma, 1989).

3.2. Set–up for normal scintillation bandwidth measurements

This set–up is straight forward. All the signals to be analyzed are filtered, using

6th–order Chebyshev anti–aliasing filters and then are fed to the analogue to digital converter (ADC) of the computer as shown in Fig. 3.1. This set–up is useful for the analysis of data obtained during clear–sky conditions, in case one is interested only in the high frequency ($> 10^{-2}$ Hz) spectral components, in order to determine the upper corner frequency and the spectral slope.

For this configuration a sampling frequency of 45 Hz is chosen. The cut–off frequency of the analogue low–pass filters is set to 20 Hz. After analogue to digital conversion, the sampled signals are decimated to 2.5 Hz using a 81–tap low–pass digital filter. The ripple introduced by this digital filter is less than that due to the analogue filter (0.1 dB). To obtain sufficient statistical reliability, four segments of data, each consisting of 1024 data samples (after decimation), are acquired in a time period of 27.3 minutes. With the effective sampling frequency of 2.5 Hz, spectral information in the scintillation bandwidth of 2.44×10^{-3} Hz to 1.2 Hz can be obtained, using a standard fast Fourier transform procedure. The reason for selecting this lower frequency end is to have more spectral components in the flat part of the spectrum, so that the corner frequency can be estimated more reliably. From the same calculated data, variance, autocorrelation function, probability density and distribution functions can be obtained. In the case of dual radio frequency signal analysis it is also possible to compute the cross–correlation function, cross–spectral density function, coherence and spectral ratio.

3.3. Set–up for wide scintillation bandwidth measurements

The set–up in this case is similar to the previous one but with variable cut–off frequency filters (see Fig. 3.2). Taking all the relevant points, such as adverse weather conditions, into consideration, the lowest and highest scintillation frequencies of interest for the OPEX are selected as 4×10^{-4} and 20 Hz respectively (see Sec. 2.4).

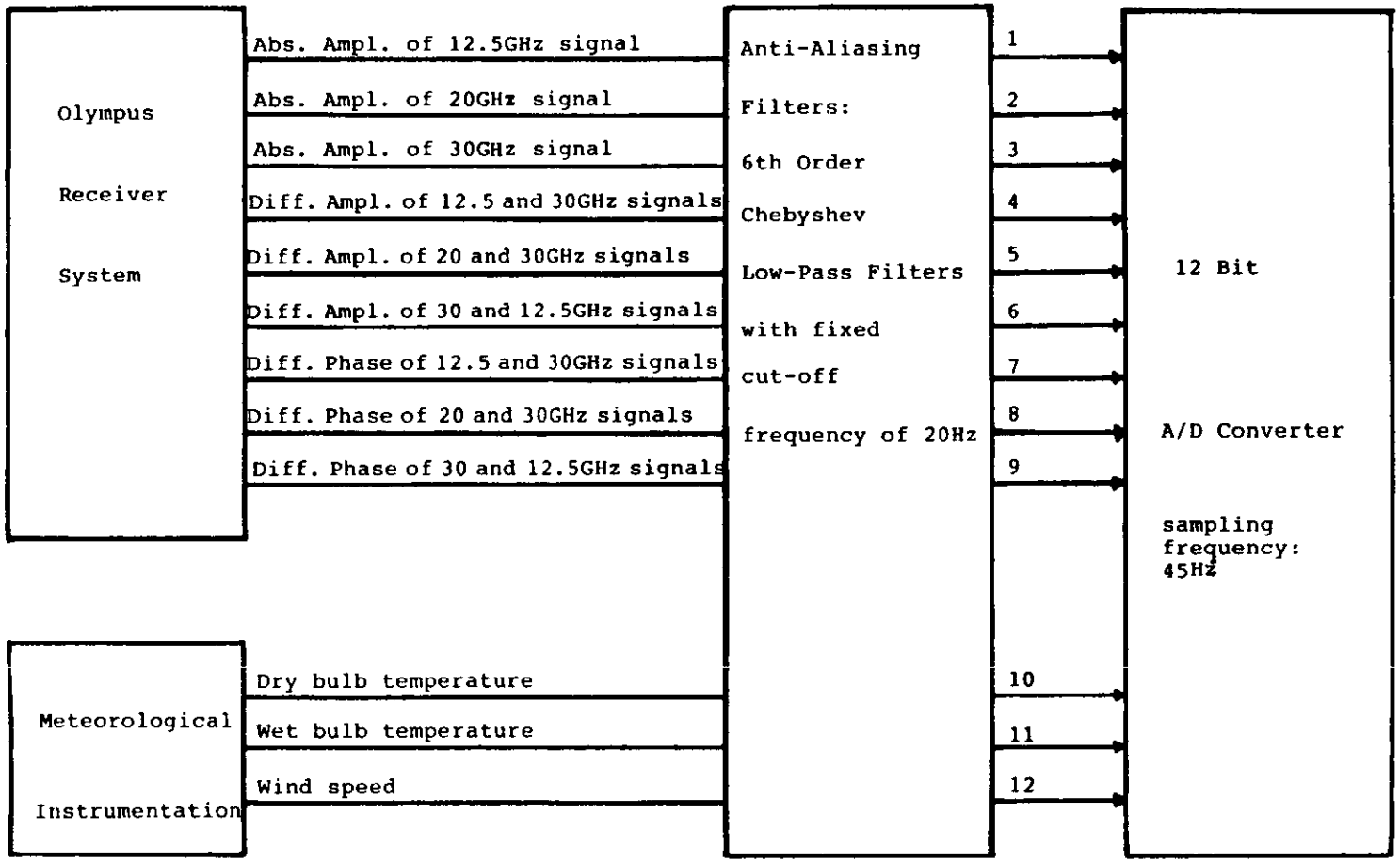

Figure 3.1 Data acquisition system for normal scintillation bandwidth (2.44×10^{-3}Hz to 1.25Hz) analysis.

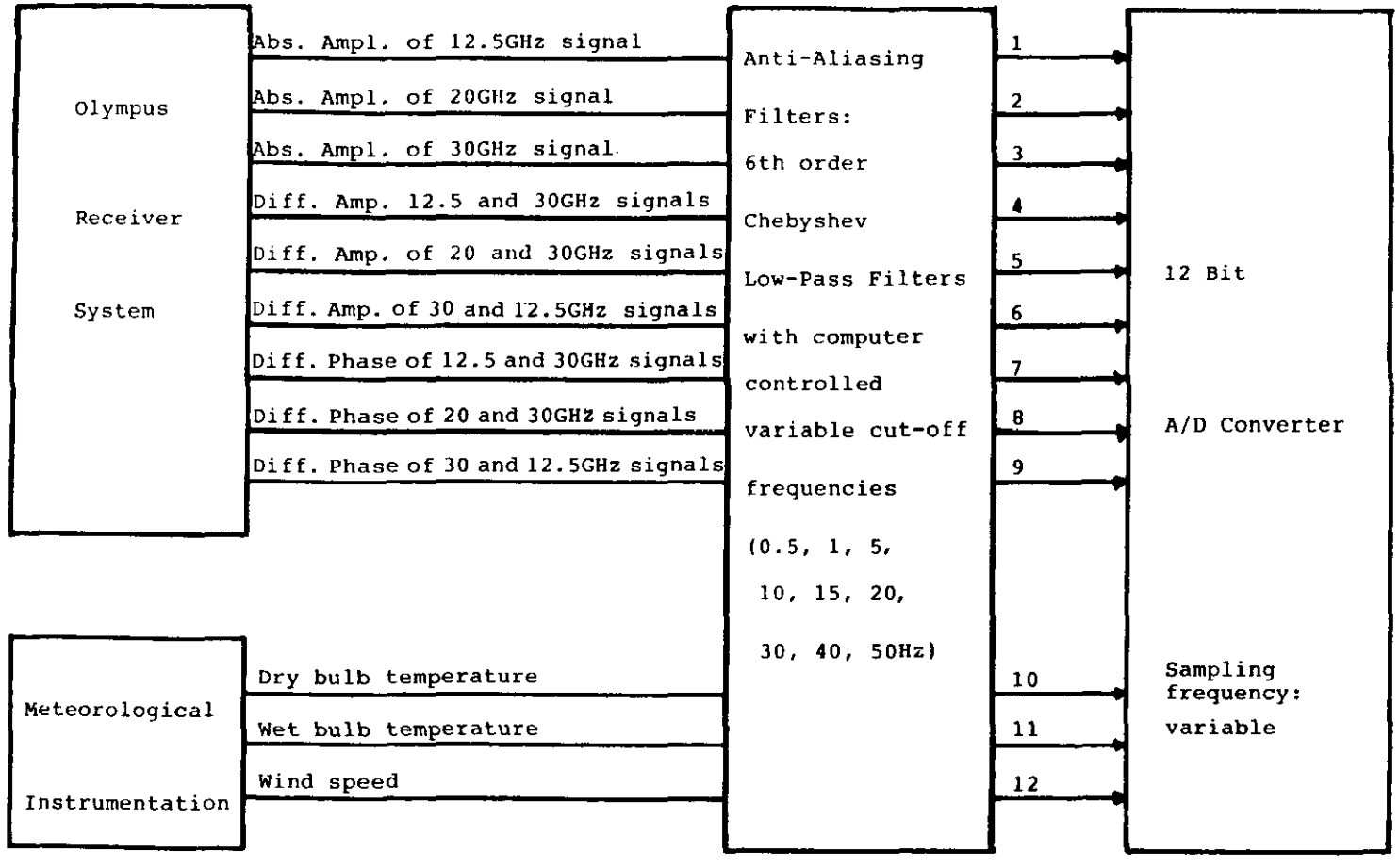

Figure 3.2 Data acquisition system for wide scintillation bandwidth (4×10^{-4}Hz to 20Hz) analysis.

As it is necessary to have such a wide scintillation bandwidth, it is not possible to obtain all the frequency components by analyzing just one segment of data points (1024). Therefore, it is usual practice to provide the scintillation spectrum into two or more somewhat overlapping frequency regions. The whole bandwidth of interest can be covered by sampling the signal at 45 Hz and to obtain the lower part of the frequency spectrum, the sampled data can be decimated.

To achieve a reasonable statistical reliability, four segments of data are to be taken for each part of spectrum. That is, the signal is to be sampled at 45 Hz for about 2.8 hours. Storing and preprocessing of this large amount of data, especially when multiple number of signals are involved, requires much computer memory space and also lot of computer time. To avoid this cumbersome procedure, a method is developed that makes use of a 6th–order Chebyshev anti–aliasing filter (with a pass–band ripple of 0.1 dB and a slope of 46 dB/octave) with a computer controlled variable cut–off frequency depending on the actual sampling frequency.

In the prototype design there are nine variable cut–off frequencies available on two separate printed boards. The upper 7 cut–off frequencies (50, 40, 30, 20, 15, 10 and 5 Hz) are accommodated on one board and the lower two (1 and 0.5 Hz) are on the other board. The cut–off frequencies can be changed by switching from one set of resistors to another set of resistors on each board. The switching is controlled by a computer output which is programmed by software.

To cover the above mentioned scintillation bandwidth and to have a reasonable statistical reliability four segments of data are to be collected at a sampling frequency of 45 Hz (f_{s1}). For this data collection the cut–off frequency of the anti–aliasing filter is to be set at 20 Hz. Next, the cut–off frequency of the filter is to be switched to 5 Hz and the sampling frequency to 11 Hz (f_{s2}) for the collection of four segments of data. Finally, the cut–off frequency is to be set to 0.5 Hz and the sampling frequency to 2 Hz (f_{s3}). However, this time initially 20 segments of data are acquired. For the sole

purpose of checking the stationarity, all 28 segments of data from the three sampling frequencies are decimated by simply ignoring the in between samples, to obtain an effective sampling frequency of 1 Hz without averaging or filtering. Thus, 91,372 and 2048 samples are obtained from the three sets of data respectively. The time difference between these three sets of data is assumed to be 1 second (the delays introduced by filter switches, decoder and the sampling frequency switching mechanism of the computer are taken into account). This total of 2511 data samples is divided into 78 parts, each consisting of 32 samples. Each part is considered independent and checked for stationarity at 5% level of significance using standard procedures (Bendat and Piersol, 1971). Data which is not stationary at the 5% level of significance are ignored. The 20 segments of data obtained at 2 Hz sampling frequency are decimated to four segments of data to obtain an effective sampling frequency of 0.4 Hz using a 61–tap low–pass digital filter (the transition region of the filter starts at 0.18 Hz and ends at 0.25 Hz). The ripple introduced by this filter is less than 0.1 dB and can be neglected when compared with the passband ripple of the analogue filter.

By use of this method, three sets of data, each consisting of four segments are obtained. Again, each set of data is checked for stationarity at 5% level of significance, individually following the procedures cited above. This second check is carried out as a subroutine procedure. The reason for this is that in the analysis programs, a provision is incorporated to perform the stationarity check automatically before calculating the FFT of the input data. Then, each segment of data is used to calculate the spectral density function at the scintillation frequency components by using standard FFT routines. Without the variable filter, 466 segments of data are to be preprocessed to get similar spectra if the signal is sampled at a constant sampling frequency of 45 Hz. By use of the proposed method, the data for preprocessing are reduced to 28 segments. In this way, data reduction by a factor of up to 16 can be achieved for every channel (while the same statistical reliability is retained). Depending on the application and

necessity, the cut–off frequencies and the sampling frequencies can be selected. More details on this set–up are available elsewhere (Sarma and Herben, 1989).

3.4. A logic circuit to sample scintillation events at chosen time intervals

A logic circuit is developed to sample millimeter wave scintillation events at chosen time intervals automatically. The circuit is most helpful for the data acquisition of scintillation signals especially during weekends with little or no operator intervention.

The logic circuit for automatic sampling of scintillation events at regular time intervals is presented in Fig. 3.3. The circuit consists of an event meter, a timer and an overflow meter. It is connected with three input ports (pins 0, 1 and 2) and two output ports (pins 4 and 5) of the I/O card of the computer. The circuit operation is as follows:

Event meter: If the incoming signal exceeds a particular level, the logic output of the circuit component becomes 1. The threshold level can be adjusted depending upon the requirements. When the logic output of the event meter is 1, the computer senses this through its I/O card and starts sampling. Then, the computer sends a signal through its I/O card, both to the "sampling indicator light emitting diode (LED)" and to the timer. When the logic is high the timer resets. When the sampling is completed the "event acknowledge logic" becomes low and subsequently the timer starts and the yellow LED is switched off.

The timer: With its RC components the timer can be set between 0.5 and 50 hours. Initially, the output of the timer is low. When the "set time" is reached, the logic output becomes high. When the logic output of both the timer and the event meter are high, the flip–flops logic output becomes high and subsequently the computer starts sampling again. Initially, the ADC looks at pin 2 of the I/O card. However, for the second sampling the ADC looks at pin 0 and ignores pin 2.

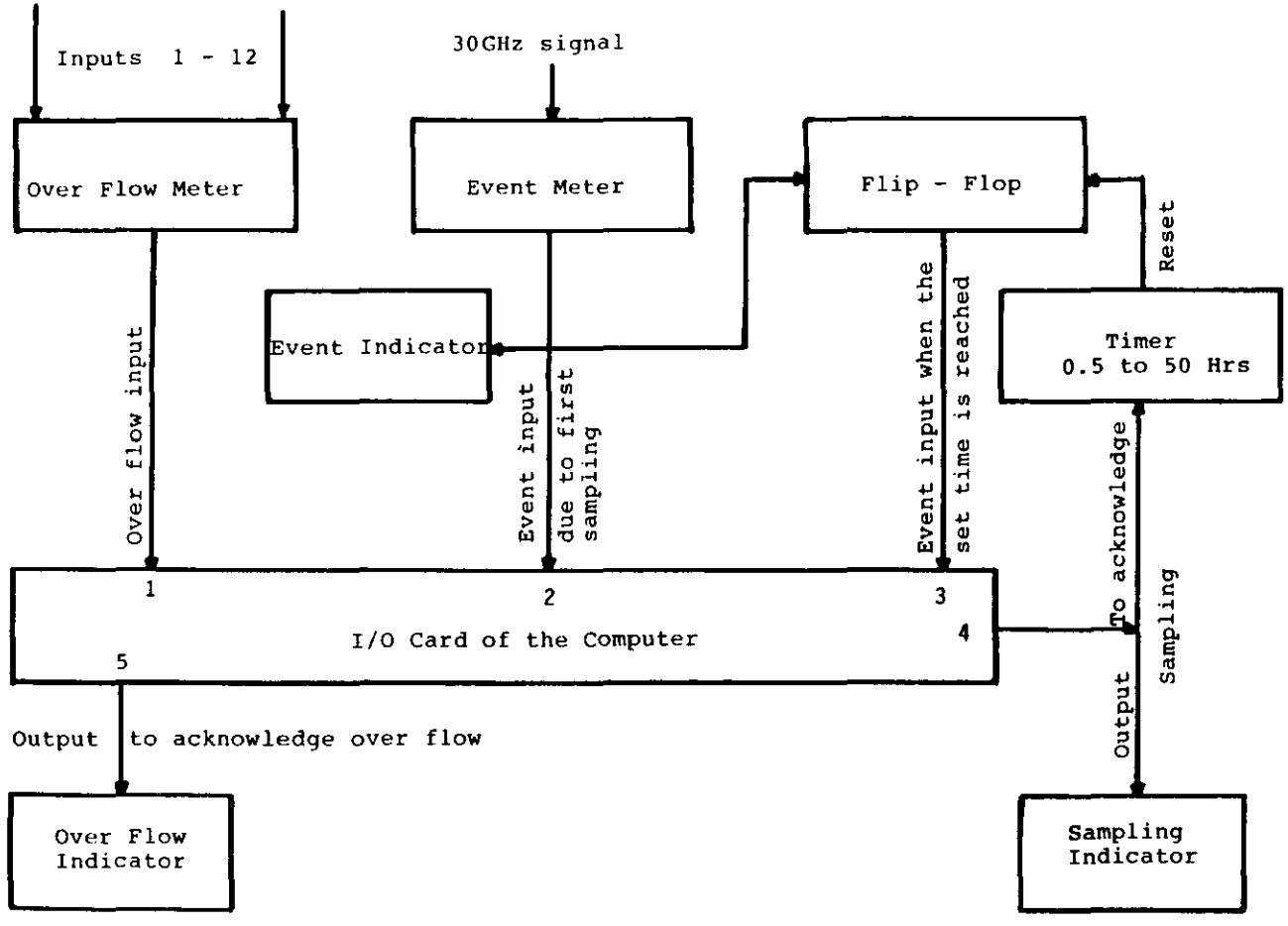

Figure 3.3 A logic circuit to start the sampling of "scintillation events" at chosen time intervals.

The main purpose of the timer is to avoid a sampling restart immediately after one sampling period is over and to wait for a fixed time interval to start again when there is an event.

The overflow meter: This circuit component consists of two 7427 IC's and one 7410 IC to accommodate 12 input channels. When one of the input signals exceeds a particular level, in the present case 10 V, the output from the overflow meter becomes high. The computer recognises this through pin 1 of the I/O card and activates, through pin 5, the "overflow indicator LED" and also resets the flip–flop. The Analogue to Digital (A/D) conversion program looks at pin 1 of the I/O at every block of 2048 data samples and when the logic is high the program stops the conversion, indicating that there is an overflow. The overflow meter has a provision for variable threshold between 0 and 10 V. The working principle of the logic circuit is illustrated in Fig. 3.4.

A computer program is written to operate the hardware logic circuit. In this, a provision is made so that data will be stored only when the variance of the incoming signal exceeds a given threshold.

The program operates as follows: Whenever the amplitude of the incoming signal exceeds a given threshold set by the hardware logic circuit, the program activates the A/D converter. Initially, the program samples about 1/4 of the required total sampling period to check whether the signal enhancement is due to tropospheric turbulence, drift in the receiver, or some other reason. To identify the scintillation event correctly the program computes the variance of the sampled data. When this variance exceeds a given threshold set by the program, then only it continues sampling for a complete sampling period.

3.5. Humidity sensor

A common way to determine the humidity is to measure the cooling effect produced

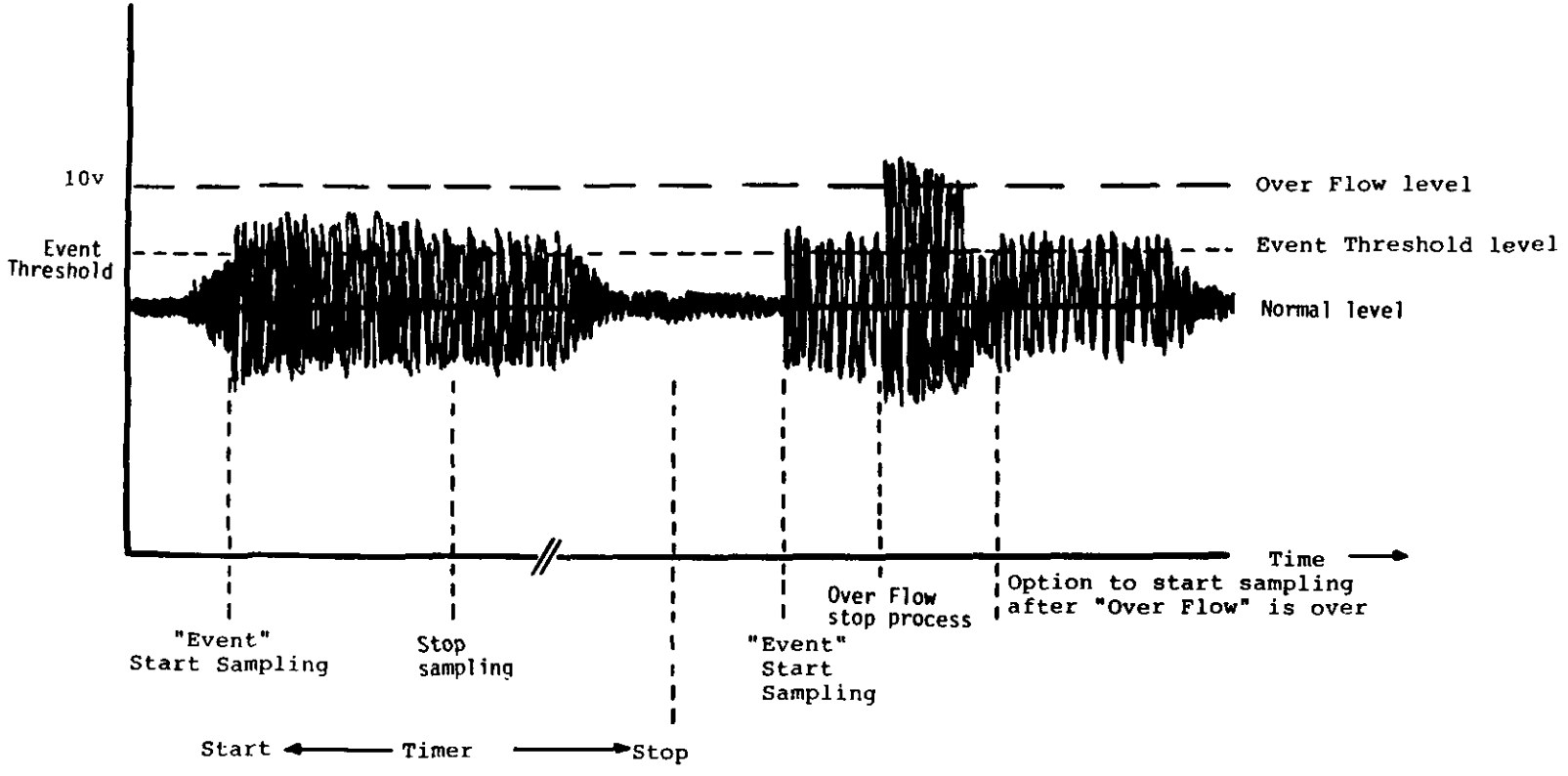

Figure 3.4 Illustration of "Start Sampling Events" with the logic circuit

by evaporating water from a wick (supplied by a distilled water bottle containing an inlet for free airflow) surrounding a thermistor bead. Two thermistor beads (ITT U 23) are used for the measurement of both dry and wet bulb temperatures (T_{wet} and T_{dry}). To linearize the response of the thermistor, a linearizer circuit is developed based on a recently published linearizer circuit (Khan, 1985). By use of this circuit and by dividing the whole temperature range of interest into six subranges, an accuracy better than 0.01°C in temperature and 0.04 mb in humidity is achieved. The details about the circuit are given elsewhere (Sarma and Herben, 1989).

The partial water vapour pressure e (humidity) can be calculated from the measured T_{wet} and T_{dry}, using the following formulas (Fleagle and Businger, 1963):

$$e = e_s - 0.666\,(T_{dry} - T_{wet}) \tag{3.1}$$

where $e_s = 10^{[9.4051-2353/T_{dry}]}$ is the saturation water vapour pressure.
Both e and e_s are in millibars; T_{dry} and T_{wet} are in Kelvin. The refractive index n can be obtained from e and T_{dry} using the formula

$$n = (77.6/T_{dry})\times(1013.25+4810\ e/T_{dry}) \tag{3.2}$$

A provision is made to attach the atmospheric turbulence probe to the wind vane so that the temperature sensors always face the direction of the incoming wind. The wind vane is placed high enough above the ground to avoid any local turbulence caused by the proximity of the surrounding obstacles (Helmis et al., 1983).

3.6. Preprocessing of data

Once the data have been digitised, certain operations have to be performed on the

acquired data before they are processed to improve the accuracy of the results. These operations involve the application of digital filtering techniques, detection and removal of dc levels and possible trends, and checking for stationarity. All these operations are discussed briefly in the following sections. The block diagram of 'signal processing' steps is shown in Fig. 3.5; whereas details of computer programs for signal processing can be found elsewhere (Sarma, 1988).

3.6.1. Digital filtering

Digital filters are used in signal processing for a number of reasons, including the following:

a) Smoothing of data

b) Evaluation of properties in various frequency bands of interest

c) Signal to noise ratio improvement.

In the present work the "optimal, equi–ripple linear phase design technique" (Peled and Liu, 1976) is used in developing a non–recursive digital filter. Depending upon the number of iterations used, any desired accuracy can be realised. With this technique both low and high–pass filters can be developed, from which band–pass filters can be deduced.

3.6.2. Calibration procedures

The process of recording signals is relatively simple. The real problem lies in ascribing the physical units. It is the usual procedure to express spectral densities of the EM wave scintillations of the beacon signals in terms of dB^2/Hz. Hence, the amplitude of the EM signals are converted to decibels before being processed. Similarly, the differential phase signals, temperature signals and wind speed signal are converted

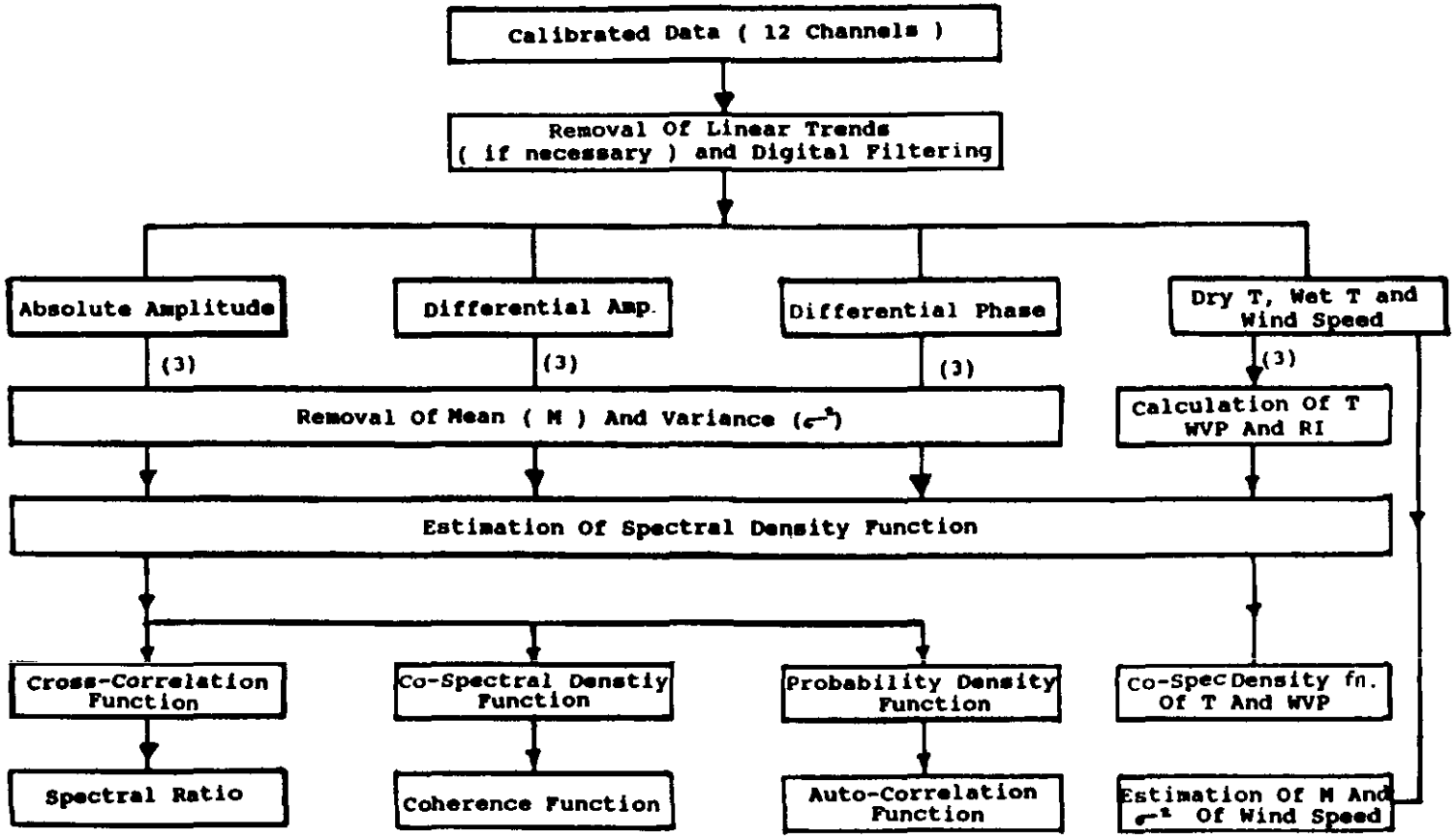

Figure 3.5 Block diagram of 'signal processing ' steps

T: Temperature
WVP: Water vapour pressure
RI: Refractive Index

into radians, centigrade and meters/second, respectively. It is convenient and time saving to incorporate the calibration procedures in the computer program that filters the sampled data.

3.6.3. Trend removal

Sometimes the acquired data may have some imperfections due to a linear or slowly varying trend accompanying the particular time period of interest. The data is said to have a trend if they have a frequency component with a period that is longer than the record length. Such linear trends are expected occasionally, for instance due to drifting of the satellite. Trend removal is an important intermediate step in the digital processing of random data. If trends are not removed from the data, they can completely nullify the estimation of the low frequency spectral content. The application of high–pass digital filters does not solve this problem. Either least–squares or average slope method is to be used. A least–squares method is preferred because of its better accuracy (Bendat and Piersol, 1971). Trend removal operations are to be performed only if trends are to be expected in the data. Otherwise extra noise will be introduced at the low frequencies.

3.6.4. Test for stationarity

For signal analysis of propagation data, the sampled data are assumed to be stationary and ergodic. This assumption may not always be true for various reasons, such as a variation of meteorological circumstances during the record time or malfunction of any component in the receiver. To acertain the stationarity, the sampled data should qualify the following:

a) In the case of non–stationarity, the sampled record should be able to properly reflect

the nonstationary character of the data.

b) The sampled record should be long compared with the lowest frequency component present in the data.

c) Time trends in the mean square value of the data should reveal the non–stationarity if present.

When once the data are qualified, the stationarity test can be performed in various ways. The reverse arrangement test is followed for this purpose. The advantage of this method is that the data need not to be free from periodicities (Bendat and Piersol, 1971). One exception to this is that the fundamental period should be short compared with the averaging time used to compute the sample values.

3.7. Single–signal frequency analysis

In EM wave propagation research, spectral analysis using a Fast Fourier Transform (FFT) algorithm is very important. This gives a clear picture of the frequency composition of the signal, which describes the basic characteristics of the received EM wave. Several FFT algorithms are available. One is an FFT algorithm due to Bringham (1974). Another is the one described by Ferguson (1982). Relatively, the former requires less computer working space, whereas the latter is more efficient in terms of computer time. If sufficient computer working space is available, the algorithm due to Ferguson is recommended.

To reduce the leakage problem, which is inherent in the discrete Fourier transform, a cosine tapering (Bingham, 1967) is used in the present work. Both frequency smoothing and segment averaging are performed to improve statistical reliability. As most of the spectra of both the EM wave and meteorological data show definite slopes (on a logarithmic scale, in particular frequency regions and depending upon the weather conditions), a simple subroutine is incorporated in the FFT computer program to

calculate automatically the spectral slope between any two frequencies. To avoid confusion, this should be followed by a manual check of the spectral plots.

The variance is estimated using both the time samples and the computed frequency spectrum. These two variances are cross–checked against each other to make sure that the analysis is correct.

3.7.1. Estimation of autocorrelation function

Estimation of the autocorrelation function of the radio signals helps in detecting possible signal periodicities. These periodicities could for instance be caused by the movements of antenna structures. In the signal analysis (see Chapter 4), the average spectral density function corresponds to 1024 data points. To observe any trends in the autocorrelation function, it is usually sufficient to take 1/4 of 1024 as the maximum lag number. The autocorrelation function estimation can be done in two ways by the direct method and by the FFT method. The first is relatively easy to understand; the second one is more efficient. The second is recommended for the data analysis.

3.7.2. Functions related to probability distribution

Analysis of the slow changes in the signal amplitude due to tropospheric scatter indicates that the signal amplitude has a logarithmically normal probability distribution; therefore, the radio signals are analyzed with respect to this distribution. The probability density and cumulative distribution functions of every set of radio data are computed and compared with the theoretical values. For general understanding of the signal behaviour some histograms are built up.

Normalisation of the probability density function is achieved by multiplication with the width of the class intervals. To measure the total discrepancy between the

measured and theoretical probability density functions, the squares of the discrepancies in each class interval are normalised by the associated expected frequencies and summed to obtain the sample statistics. This is known as the chi–square sum, which can be used to determine at what level the hypothesis is accepted or rejected from standard statistical tables. The formula to be used is

$$\chi^2 = \sum_{i=1}^{k} \frac{(f_i - F_i)^2}{F_i}$$

where f_i is called "observed frequency" in the i^{th} class interval and F_i is the number of observations that would be expected to fall within the i^{th} class interval if the true probability density function of χ equals the theoretical one.

3.8. Dual–signal frequency analysis

In the communication field it is very important to know the general dependence of the values of one set of data on the other. Once the general dependence is known, it is possible to establish at which signal fluctuation frequencies the two signals behave either similarly or dissimilarly. This information can be used for predicting the coherence bandwidth.

Dual frequency measurements have some additional advantages, compared with single frequency measurements. For example, differential phase measurements will eliminate or reduce the errors due to oscillator drifts or antenna structure movements while retaining the turbulence induced effects. The cross–correlation, cross–spectral density and coherence functions are estimated by using the standard algorithms described by Bendat and Piersol (1971). These estimations help to understand to what extent the signals at two different radio frequencies are correlated by the propagation medium. Suppose the signals are highly correlated, then it is possible to predict the

behaviour of the signal at one radio frequency from propagation measurements at the other frequency.

3.9. Plotting and storage of end results

Great importance is given to supplying each record with sufficient information to identify the record itself and to distinguish it from other records.

For exact identification of any record a format is developed giving general information such as date, time, number of channels sampled, sampling frequency, experiment number, number of samples (after preprocessing) and number of segments. This information is common to all channels recorded at the same time. An additional format of six variables gives specific information about the data in the record. For example, the power spectral density function record of a beacon signal gives information about the mean, variance, spectral slope, number of spectral points, identification code for description of the plot and identification code to store all the end results in one big file. When a graphic plot is made, both formats will be printed above the plot, making the interpretation of the results easy.

4. TYPICAL EXPERIMENTAL RESULTS

4.1. Introduction

This chapter presents some experimental results of the amplitude characteristics of the 11.5 GHz beacon signal from the European Communication Satellite (ECS) and some meteorological measurement results. The measured signals were analysed, producing the spectral density function, autocorrelation function, probability density function of the ECS beacon signal and the spectral density function of temperature, partial water vapour pressure and refractive index. The aim of presenting these results is to check the computer programs that were developed using the theory described in the previous chapter and to prove that they can be used for the Olympus satellite propagation experiments also.

4.2. Amplitude measurements of 11.5 GHz ECS beacon signal

The amplitude signal is analyzed both in normal scintillation bandwidth and wide scintillation bandwidth, using the experimental set–ups described in chapter 3. Whenever there is a change in the atmospheric conditions, the transfer function of the propagation medium will change too.

There are two types of changes in atmospheric conditions (Ishimaru, 1978):

1 Relatively long term variations (with a periodicity greater than hundreds of seconds), which tend to occur uniformly over the path. These are due to weather fronts and diurnal, seasonal and annual changes in barometric pressure, temperature and partial water vapour pressure.

2 The short–term fluctuations (with a periodicity of tenths to tens of seconds), which are associated with spatial variations of the refractive index in the millimetre to

hundred metre range. These variations are due to turbulence.

4.2.1. Normal scintillation bandwidth measurements

Several experiments were done using the experimental set–up described in Sec. 3.2. The variance of the 11.5 GHz beacon signal amplitude is obtained for each data segment consisting of 1024 data values sampled at an effective sampling frequency of 2.5 Hz. Hence, the variances correspond to a frequency range of 2.44×10^{-3} Hz to 1.25 Hz. The obtained data are processed to obtain the spectral density function, auto–correlation function and probability density function. Typical representation of these functions are shown in Figs. 4.1, 4.2 and 4.3.

The amplitude spectrum (Fig. 4.1) shows a frequency independent horizontal portion in the low frequency region and a steep slope in the high frequency region. The lowest frequency component in the figure has an enhanced spectral density. This could be due to absorption or to drift in the receiver system. The cause is to be investigated thoroughly after analysis of many scintillation events obtained during different meteorological conditions. Anyway, the lowest eight spectral components are less reliable, compared with the rest of the components. The slope in the high frequency region is steeper (~ -5.0) than expected for a point receiver (–8/3 slope). This is due to the use of a receive antenna with a large aperture (diameter = 8 m) (Herben, 1983a). When straight lines are drawn through the experimental points in both the low and high frequency regions, the corner frequency can be estimated as 0.25 Hz. By use of equation (2.6) the average wind speed transverse to the propagation path (v_t) can be calculated as ~5 m/s. In this calculation the effective length of the propagation path is assumed to be 5 km.

The refractive index structure parameter C_n^2 can be calculated from the variance of the amplitude scintillation (σ_χ^2), using formula (2.3). However, as the lowest spectral

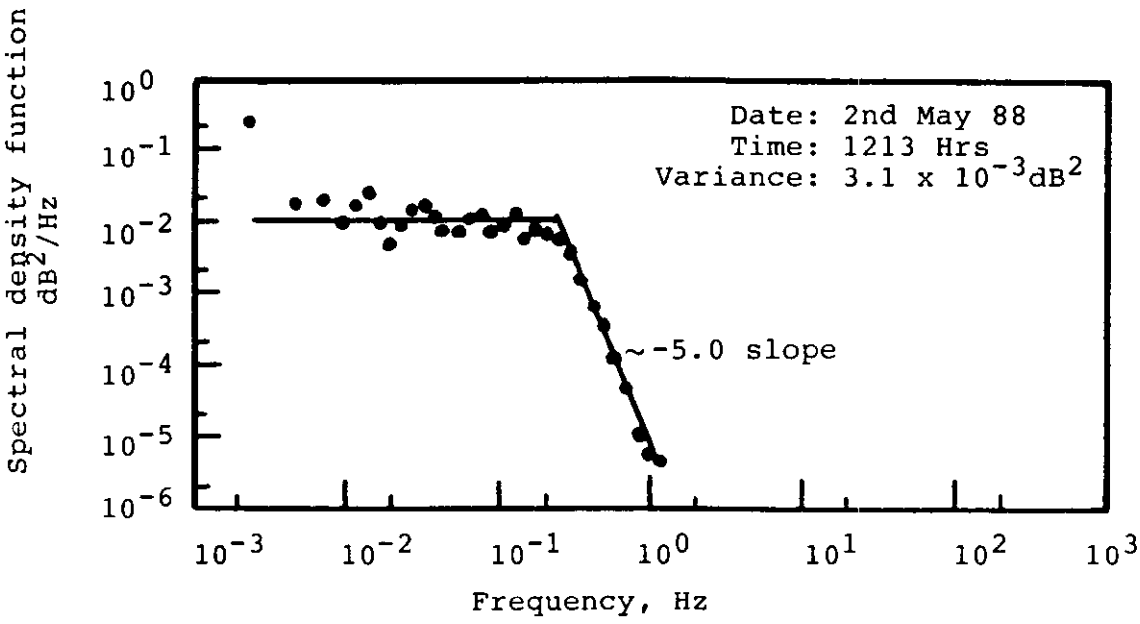

Figure 4.1 Spectral density function of the ECS beacon signal at 11.5 GHz

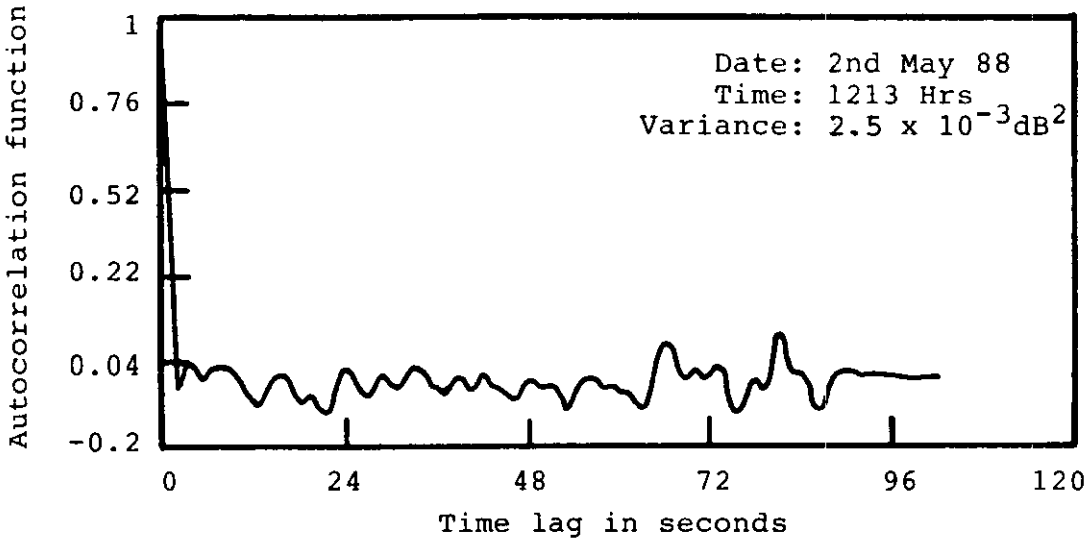

Figure 4.2 Autocorrelation function of the ECS beacon signal at 11.5 GHz

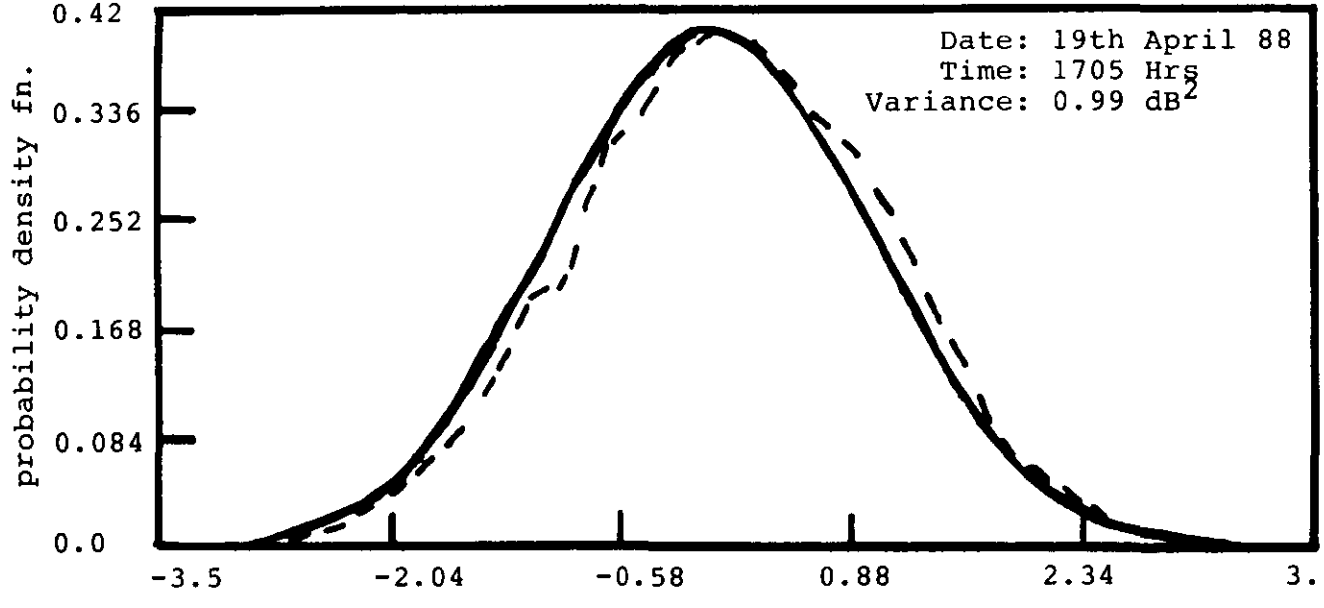

Figure 4.3 probability density function of the ECS beacon Signal at 11.5 GHz (-Theoretical,---measured)

components appear to be ambiguous, the original variance corresponding to this spectrum (3.11×10^{-3} dB^2) is to be modified. Assuming that this lowest spectral component has the same spectral density as the adjacent component in the flat part of the spectrum, the variance is adjusted by subtracting the area contributed by the ambiguous component in the "enhanced portion" of the spectrum. The modified variance is 2.83×10^{-3} dB^2. By use of this value, the C_n^2 value can be calculated as 2.52×10^{-12} $m^{-2/3}$. If v_t is obtained from other measurements, the position of the horizontal line in the spectrum can be accurately determined by substituting the values of v_t and σ_χ^2 in equation (2.3). The corner frequency estimated in this way would be more precise.

The autocorrelation function of the same data is shown in Fig. 4.2 (lag value is 256). The number of segments considered is 12. For this particular lag, the time taken for the function to fall to zero appears to be about 2.5 seconds. The zero crossings can be clearly seen in the figure also. This estimation is useful to identify possible periodicities.

The probability density function of the ECS beacon signal, taken at some other time, is shown in Fig. 4.3. As expected, the density function of the amplitude signal is log–normal. This is confirmed by the chi–square goodness–of–fit test between the experimental and theoretical distribution curves. The test gives an acceptance of the hypothesis of normality at 5% level of significance ($\chi^2 = 20$). Small discrepancies could be due to variations in the atmospheric conditions during the 27.3 min registration time. More information about the probability density functions of the data obtained from satellite links can be found elsewhere (Herben, 1983a; Moulsley et al., 1982).

4.2.2. Wide scintillation bandwidth measurements

Three sets of data, each consisting of four segments of data, are obtained using the

experimental set–up described in chapter 3. The collected data are checked for stationarity. Then, each segment of data is used to calculate the spectral density function at the scintillation frequency components by using standard FFT routines. Later, segment averaging and frequency smoothing are applied to each set of results to improve the statistical reliability.

Logarithmic frequency smoothing grouping variable number of frequency components; i.e., except for the first eight frequency components the rest of the components are grouped into six blocks; the number of the components in each block increases by a power of 2 followed by averaging to obtain four components from each block. When logarithmic smoothing is applied, each set results in 32 spectral points with varying statistical reliability. The 90% confidence interval for the first 8 lowest frequency components is given by $0.52\ \hat{G}(f) < G(f) < 2.93\ \hat{G}(f)$, where $\hat{G}(f)$ is the spectral density estimate and G(f) is the true spectral density (Bendat and Piersol, 1971). While for the highest frequency estimates the 90% confidence interval is better than $0.82\ \hat{G}(f) < G(f) < 1.24\ \hat{G}(f)$. That is, the high frequency components have better reliability compared with the low frequency points. Because of partial overlapping of three sets of results a better smoothed spectrum can be achieved by considering the points of highest reliability in the overlapped regions.

A typical amplitude scintillation spectrum, obtained in this way, is shown in Fig. 4.4. In this particular example, the spectral components above 2 Hz are masked by the system noise. This need not be the case for other experiments such as OPEX. The three portions of the spectrum contributed by three sets of data are marked along with the region where the aliasing error (due to first set) is greater than the passband ripple of the analogue filter. The aliasing error in amplitude due to first set below ~9 Hz is less than 0.1 dB; in the second case the aliasing error below ~2 Hz is less than 0.1 dB; in the third case the aliasing error below ~0.15 Hz is less than 0.1 dB. In these figures it is assumed that the spectra in the aliased regions are flat. If the spectral components

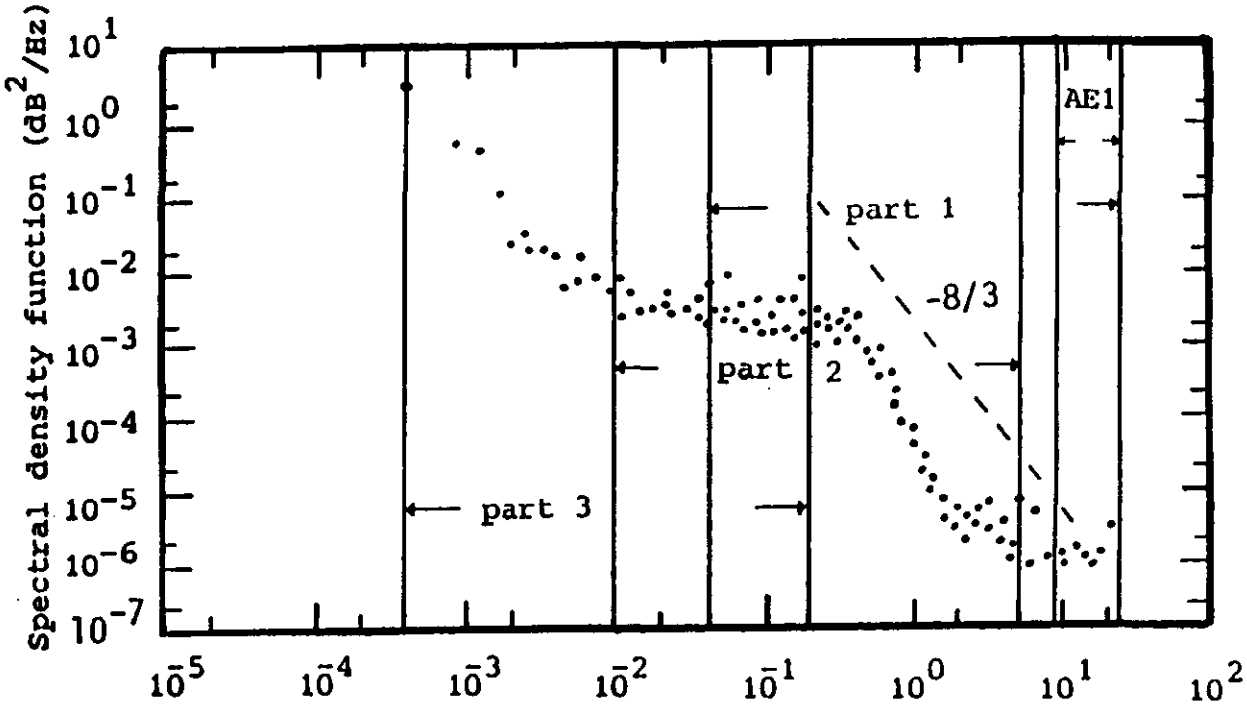

Fig. 4.4 Spectral density function of amplitude scintillations at 11.5GHz

(Date:11th Feb.88; starting time: 12:50 GMT)

part 1: Due to first data set (f_{s1})

part 2: Due to 2nd data set (f_{s2})

part 3: due to 3rd data set (f_{s3})

AE1: Aliased region where the error > the ripple of the filter due to f_{s1}

above 2 Hz are not masked by system noise, further reduction in the aliasing error in the first two parts of the spectrum is possible because of the –8/3 decrease with frequency in the high frequency region of the spectrum.

The reason for not selecting an analogue filter with a cut–off frequency of about 0.2 Hz to obtain the third part of the spectrum is that it is relatively difficult to realise a variable cut–off frequency filter extended to such a low cut–off frequency.

There are two slopes in the amplitude scintillation spectrum shown in Fig. 4.4, one in the low frequency region and the other in the high frequency region separated by a horizontal portion. The high frequency slope is, as expected due to tropospheric scattering. The enhancement in the low frequency region could be due to passing clouds during this experimental run. Usually a –8/3 high frequency slope is expected, but the steeper slope appearing in the figure is, as stated earlier, due to the averaging effect of the 8 m receive antenna aperture (Herben, 1983a).

4.3. Meteorological measurements

Measurement of meteorological parameters is important in assessing their effect on millimeter wave propagation. Once their effect is well established, weather parameters such as the average refractive index structure parameter or mean wind velocity seen by the link along the path can be accurately calculated from the radio data, which is useful in remote sensing (Herben and Kohsiek, 1984; Kohsiek and Herben, 1983).

The most important meteorological parameters such as temperature, water vapour pressure and refractive index are measured using the atmospheric turbulence probe described in chapter 3.5, and the spectra of these parameters are shown in the Figs. 4.5 – 4.7. These estimated values give very valuable information regarding the turbulent behaviour of the troposphere.

Gossard (1960) suggested that the temperature–humidity cospectrum may influence

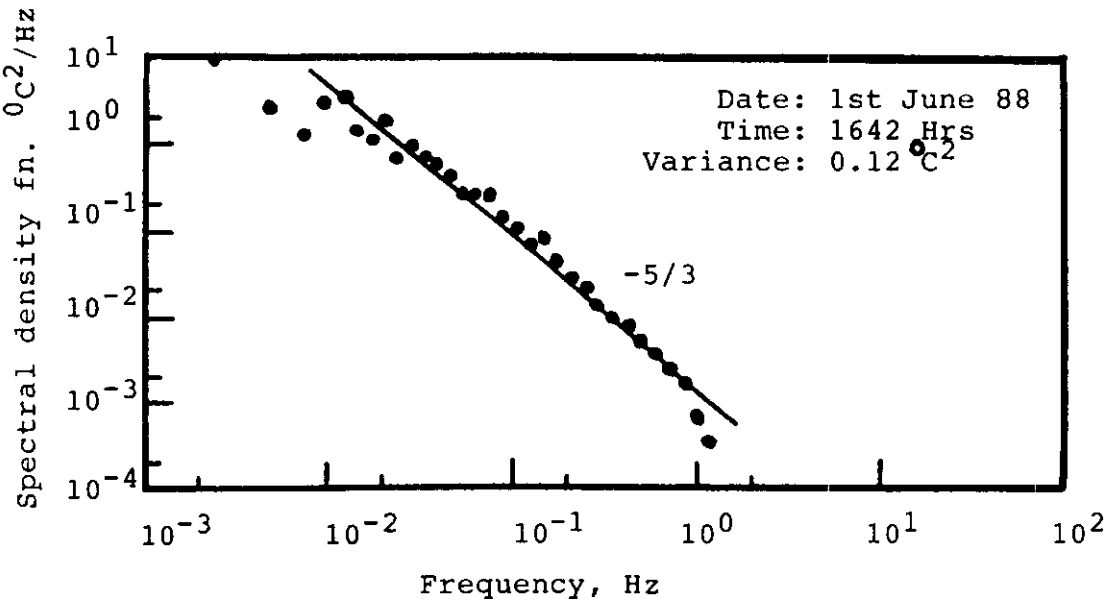

Figure 4.5 spectral density function of dry bulb temperature

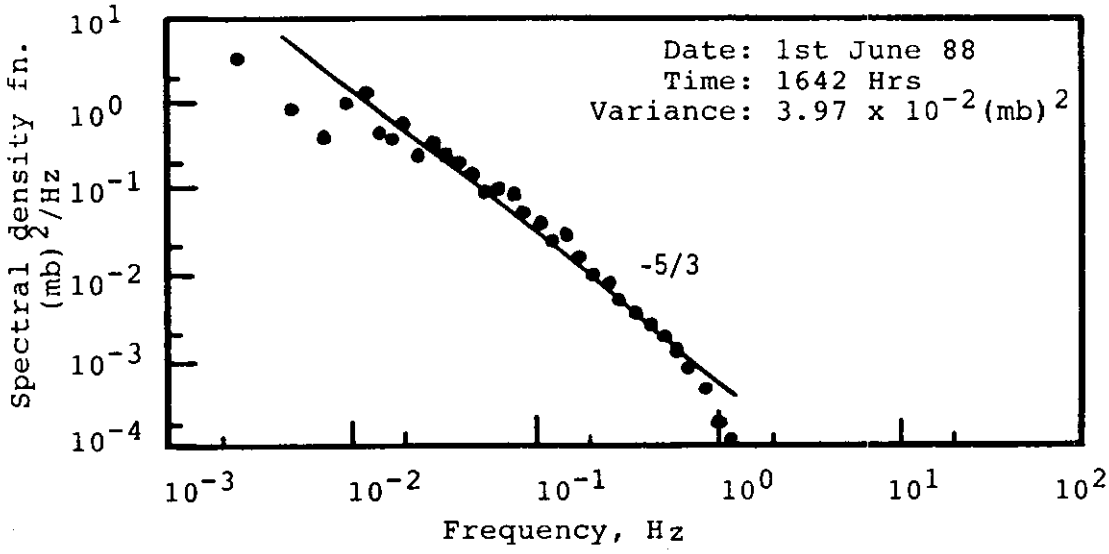

Figure 4.6 spectral density function of partial water vapour pressure

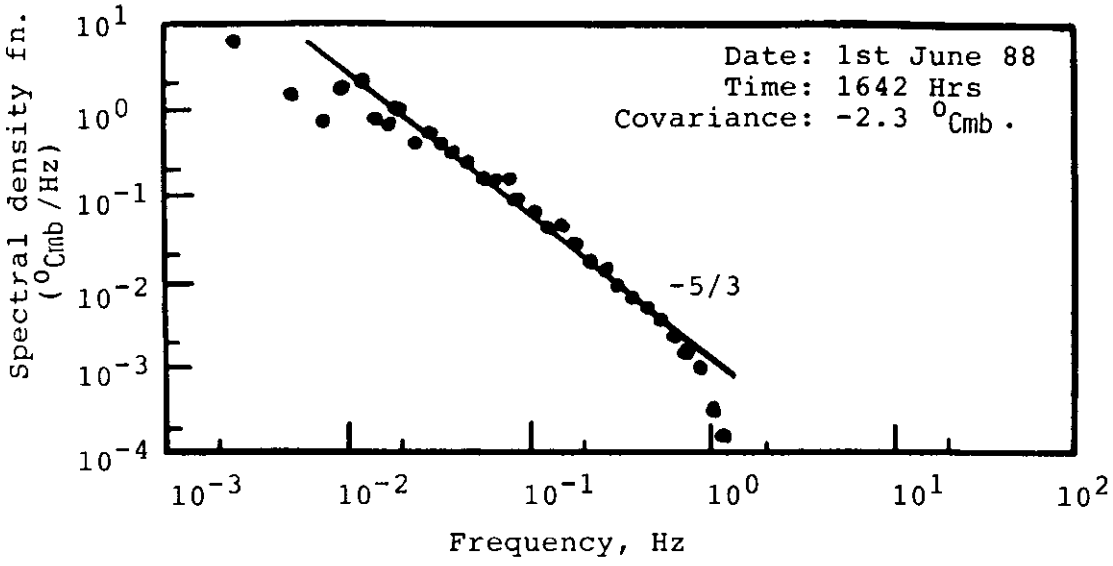

Figure 4.7 Co-spectral density function of dry temperature and partial water vapour pressure.

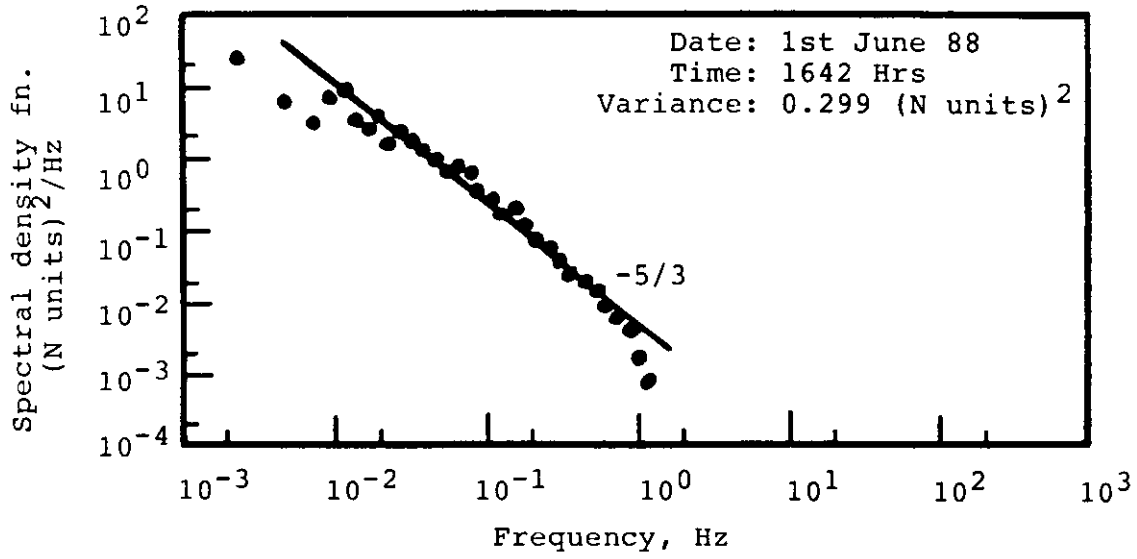

Figure 4.8 Spectral density function of refractive index.

the shape of the refractive index spectrum, especially under unstable conditions. Friehe et al. (1975) indicated that the humidity fluctuations may be important in the cases with a significant moisture flux from the ground. In the analysis of the refractive index spectrum, the contribution of the cospectrum of temperature and humidity is often not negligible, especially when the cospectrum changes sign. This implies that the spectrum of refractive index need not be identical in shape to that of the temperature and humidity even if the latter two have the same spectral shape. Power spectra obtained under unstable conditions differ significantly at the lower frequencies from those obtained within a stable layer, although both are seen to approach a –5/3 slope at the higher frequencies.

The correlation between temperature and humidity fluctuations can be quantified using the correlation coefficient defined as

$$\rho_{eT} = \frac{\sigma_{eT}}{\sqrt{\sigma_T^2 \, \sigma_e^2}} \tag{4.1}$$

where σ_T^2 and σ_e^2 are the variances of temperature and humidity fluctuations and σ_{eT} is the covariance of these two. Substituting $\sigma_T^2 = 177.0\times10^{-3}$ C^2, $\sigma_e^2 = 39.7\times10^{-3}$ $(mb)^2$ and $\sigma_{eT} = 68.4\times10^{-3}$ C mb (obtained from the plots presented in Figs. 4.5–4.7) in the above equation, ρ_{eT} appears to approximate unity. This agrees with the atmospheric conditions during the experiment, which were very stable. One hour before this particular record was obtained, the sky was cloudy and it was raining slightly. All the spectra shown in Figs. 4.5–4.8 exhibit the –5/3 slope in the higher frequency region. However, the two highest spectral components deviate from the –5/3 slope. Obviously this is due to instrument (atmospheric turbulence probe) lag.

The atmospheric refractive index structure parameter C_n^2 can be estimated following the equation (Ishimaru, 1978)

$$C_n^2 = \frac{13.67}{v} \left(\frac{f}{v}\right)^{-5/3} G_n(f) \qquad (4.2)$$

where $G_n(f)$ is the spectral density function of the refractive index function and v is the wind speed blowing from a given direction towards the sensor device that measures n. This equation can be applied within the frequency region of the spectrum where the theory of the Kolmogorov spectrum in the inertial subrange applies. From Fig. 4.8 it can be seen that the spectral density value at 0.59 Hz is 1×10^{-14} units^2. Assuming v = 1 m/s, the C_n^2 value can be calculated, using equation (4.2), as 32.9×10^{-4} m$^{-2/3}$.

Following Hill (1978), a relationship between the refractive index fluctuations and the temperature and water vapour pressure fluctuations can be established, neglecting the pressure fluctuations as

$$\Delta n = A_T \Delta T + A_e \Delta e \qquad (4.3)$$

where A_T and A_e are the temperature and water vapour pressure sensitivity parameters which are defined as $A_T = \frac{\partial n}{\partial T}$ and $A_e = \frac{\partial n}{\partial e}$ and depend on the radio frequency considered. In terms of average values, equation (4.3) can be written as

$$\langle \Delta n^2 \rangle = A_T^2 \langle \Delta T^2 \rangle + 2A_T A_e \langle \Delta T \Delta e \rangle + A_e^2 \langle \Delta e^2 \rangle \qquad (4.4)$$

For zero mean values of the fluctuations, equation (4.4) can be written in terms of variances as

$$\sigma_n^2 = A_T^2 \sigma_T^2 + 2A_T A_e \sigma_{eT} + A_e^2 \sigma_e^2 \qquad (4.5)$$

It is interesting to see the relative contribution of the three terms in the above equation to σ_n^2 for the meteorological conditions existing during the experiment under

discussion, viz.:

Dry temperature = 290.6 K

Partial water vapour pressure = 1.28 mb

$\sigma_T^2 = 116.8\times10^{-3}$

$\sigma_e^2 = 39.7\times10^{-3}$

$\sigma_n^2 = 29.9\times10^{-14}$

$\sigma_{eT} = 68.4\times10^{-3}$

Neglecting the frequency dependent part of the refractive index (Hill and Clifford, 1981), the values of A_T and A_e are estimated as -0.97×10^{-6} and 4.42×10^{-6}.

The relative contributions of the three terms in Eq. (4.5) to σ_n^2 are as follows:

$A_T^2\sigma_T^2/\sigma_n^2$: 0.367

$2A_TA_e\sigma_{eT}/\sigma_n^2$: –1.962

$A_e^2\sigma_e^2/\sigma_n^2$: 2.595.

The interesting point to note is that for this experiment the contribution of the temperature fluctuations to the variance of the refractive index fluctuations is small compared with the contribution of the partial water vapour pressure fluctuations. This was also found by Kohsiek and Herben (1983) for experiments at 30 GHz.

As mentioned earlier, all the spectra (Figs. 4.5–4.8) exhibit a –5/3 slope in the high frequency region. Knowing from the spectrum the minimum frequency f_0 for which the –5/3 slope applies, we can calculate the outer scale of turbulence L_0 from the approximate equation

$$L_0 \simeq \frac{v}{f_0} \tag{4.6}$$

For example, f_0 obtained from the temperature spectrum is approximately 0.028 Hz. Therefore, for v = 1 m/s, the outer scale of turbulence is about 37.5 m.

5. CONCLUSIONS AND RECOMMENDATIONS

5.1. Conclusions

The main object of the Olympus project is the evaluation of the influence of the propagation effects on the use of the 20 and 30 GHz frequency bands for future satellite communications in Europe. The aspects of the investigation include the influence of meteorological parameters such as temperature, water vapour pressure and refractive index fluctuations on radio signal scintillations. To achieve this object several computer programs have been written in Fortran language for data acquisition and signal processing of the radio beacon signals from the Olympus satellite, the meteorological signals from the atmospheric turbulence probe and the signal from the wind speed meter.

The following are the main conclusions after consideration of all the relevant aspects of the Olympus propagation experiment:

- A systematic approach for selecting baseband filters suitable for scintillation measurements showed that the choice of the filters is a compromise between accuracy, simplicity and economy, leading to the application of both analogue and digital filters.
- The selected sampling frequency should be chosen such that the quantisation noise and aliasing error are small compared with the thermal noise of the system.
- A data acquisition method involving variable cut–off frequency filters is useful to perform wide bandwidth scintillation measurements, because this method is economical in terms of computer time and memory.
- With the newly developed humidity sensor it is possible to assess the effect of tropospheric turbulence on the propagation of 20/30 GHz signals.
- The experimental results presented in this report, obtained using the 11.45 GHz

beacon signal of the European Communication Satellite and the signals from the atmospheric turbulence probe, show that the data analysis software is working well, so the same computer programs can be used for the Olympus propagation experiments.

5.2. Recommendations

- Usually, when the operating frequency is in the absorption region (for example near 60 GHz), there will be a low frequency enhancement in the amplitude scintillation spectrum. However, even when the frequency is in the non–absorption region (for example 20 and 30 GHz), there could be some enhancement in the low frequency region. This is to be investigated both theoretically and experimentally.
- An error–free experimental set–up for differential amplitude measurements is to be developed. Experimental results are to be cross–checked with those obtained from available theoretical models.
- A model should be developed for comparing C_n^2 obtained from a satellite–to–earth radio–link with the one obtained from the atmospheric turbulence probe.

References

Barton, S.K. (Ed.), "Handbook for beacon receiver design", Issue 1, Noordwijk, The Netherlands, European Space Research and Technology Centre (ESTEC), 1985. European Space Agency, Large Telecommunications Satellite Project Olympus. OPEX–Olympus Propagation Experiment.

Bendat, J.S. and Piersol, A.G., "Random Data: Analysis and measurement procedures", Wiley Interscience, New York, 1971.

Bingham, C., Godfrey, M.D. and Tukey, J.W., "Modern techniques of power spectrum estimation", IEEE Trans. Audio Electroacoust., Vol. 15, pp. 56–66, 1967.

Brigham, E.O., "The fast Fourier transform", Prentice–Hall, Englewood Cliffs, N.J., 1974.

Cole, R.S., Ho, K.L. and Mavrokoukoulakis, N.D., "The effect of outer scale of turbulence and wavelength on scintillation fading at millimeter wavelengths", IEEE Trans. Antennas and Propagation, Vol. 26, no. 5, pp. 712–715, 1978.

Cole, R.S., Sarma, A.D. and Siqueira, G.L., "Effect of meteorological conditions on scintillation fading in the oxygen absorption region", Applied Optics, Vol. 27, no. 11, pp. 2261–2265, 1988.

Crochiere, R.E. and Rabiner, L.R., "Interpolation and decimation of digital signals – A tutorial review", Proc. of the IEEE, Vol. 69, no. 3, pp. 300–331, 1981.

Ferguson, W.E., "A simple derivation of Glassoman's general N fast Fourier transform", Computers and Mathematics with Applications, Vol. 8, no. 6, pp. 401–411, 1982.

Fleagle, R.G. and Businger, J.A., "An introduction to atmospheric physics", Academic Press, New York, 1963.

Friehe, C.A., La Rue, J.C., Champagne, F.H., Gibson, C.H. and Dreyer, G.F., "Effects of temperature and humidity fluctuations on the optical refractive index in the marine boundary layer", J. Opt. Soc. Am., Vol. 65, no. 12, pp. 1502–1511, 1975.

Gossard, E.E., "Power spectra of temperature, humidity and refractive index from aircraft and tethered balloon measurements", IRE Trans. Antennas and Propagation, Vol. 8, pp. 186–201, 1960.

Gurvich, A.S., "Effect of absorption on the fluctuation in signal level during atmospheric propagation", Radio Eng. Electron. Phys., Vol. 13, no. 11, pp. 1687–1694, 1968.

Helmis, C.G., Asimakopoulos, D.N., Caroubalos, C.A., Cole, R.S., Medeiros Filho, F.C. and Jayasuriya, D.A.R., "A quantitative comparison of the refractive index structure parameters derived from the refractivity measurements and amplitude scintillation measurements at 36 GHz", IEEE Trans. Geosci. Remote Sensing, Vol. 21, no. 2, pp. 221–224, 1983.

Herben, M.H.A.J., "Amplitude scintillations on the OTS–TM/$\overline{\text{TM}}$ beacon", Archiv für Elektronik und Übertragungstechnik, Vol 37, no. 3/4, pp. 130–132, 1983a.

Herben, M.H.A.J., "Rain–induced amplitude scintillations on 8.2 km line–of–sight path at 30 GHz", Archiv für Elektronik und Übertragungstechnik, Vol. 37, no. 9/10, pp. 339–340, 1983b.

Herben, M.H.A.J. and Kohsiek, W., "A comparison of radio wave and in–situ observations of tropospheric turbulence and wind velocity", Radio Science, Vol. 19, no. 4, pp. 1057–1068, 1984.

Herben, M.H.A.J., "Spectral distribution of rain–induced amplitude and phase scintillations", Archiv für Elektronik und Übertragungstechnik, Vol. 40, no. 3, pp. 180–184, 1986.

Hill, R.J., "Spectra of fluctuations in refractivity, temperature, humidity and temperature–humidity cospectrum in the inertial and dissipation ranges", Radio Science, Vol. 13, no. 6, pp. 953–961, 1978.

Hill, R.J. and Clifford, S.F., "Contribution of water vapour monomer resonances to fluctuations of refraction and absorption for submillimeter through centimeter wavelengths", Radio Science, Vol. 16, no. 1, pp. 77–82, 1981.

Hill, R.J., Clifford, S.F., Lataitis, R.J. and Sarma, A.D., "Scintillation of millimeter–wave intensity and phase caused by turbulence and precipitation", in: Proc. AGARD 45th Symp. on Atmospheric Propagation in the UV, visible, IR and mm–wave Region and Related Systems, Copenhagen, 9–13 Oct. 1989.

Ishimaru, A., "Wave propagation and scattering in random media", Academic Press, New York, 1978.

Jayasuriya, D.A.R, Medeiros Filho, F.C. and Cole, R.S., "Scintillation fading in an absorption region", in: Proc. 2nd Int. Conf. on Antennas and Propagation, Heslington, York, 13–16 April 1981. Part 2: Propagation. London: IEE, 1981. IEE Conf. Publ. 195. Pp. 221–224.

Johnson, D.E., Johnson, J.R. and Moore, H.P., "A handbook of active filters", Prentice–Hall, Englewood Cliffs, N.J., 1980.

Khan, A.A., "An improved linear temperature/voltage converter using thermistor in logarithmic network", IEEE Trans. Instrum. Meas., Vol. 34, pp. 635–638, 1985.

Kohsiek, W. and Herben, M.H.A.J., "Evaporation derived from optical and radio–wave scintillation", Applied Optics, Vol. 22, pp. 2566–2570, 1983.

Mawira, A. (Ed), "Handbook for data preprocessing. Part 1: Theory and basic information". Issue 1. Noordwijk, The Netherlands: European Space and Technology Centre (ESTEC), 1986. European Space Agency, Large Telecommunications Satellite Project Olympus. OPEX–Olympus Propagation Experiment.

Medeiros Filho, F.C., Jayasuriya, D.A.R. and Cole, R.S., "Tropospheric effects on line–of–sight links at 36 GHz and 55 GHz", IEE Proc. F, Vol. 130, no. 7, pp. 679–687, 1983a.

Medeiros Filho, F.C., Jayasuriya, D.A.R., Cole, R.S. and Helmis, G., "Spectral density of millimeter wave amplitude scintillations in an absorption region", IEEE Trans. Antennas and Propagation, Vol. 31, no. 4, pp. 672–676, 1983b.

Moulsley, T.J. and Vilar, E., "Experimental and theoretical statistics of microwave amplitude scintillations on satellite down–links", IEEE Trans. Antennas and Propagation, Vol. 30, no. 6, pp. 1099–1106, 1982.

Moulsley, T.J., Lo, P., Haddon, J., Weaver, G. and Vilar, E., "The efficient acquisition and processing of propagation statistics", J. Instn. Electronic and Radio Engrs., Vol. 55, no. 3, pp. 97–103, 1985.

Ortgies, G., "Amplitude scintillations occurring simultaneously with rain attenuation on satellite links in the 11 GHz band", in: Proc. 4th Int. Conf. on Antennas and Propagation (ICAP 85), Coventry, 16–19 April 1985. London: IEE, 1985. Conf.Publ. 248, pp. 72–76.

Ortgies, G. and Rücker, F., "Diurnal and seasonal variations of OTS amplitude scintillations", Electronics Letters, Vol. 21, no. 4, pp. 143–144, 1985.

Ott, R.H. and Thompson, M.C. Jr., "Atmospheric amplitude spectra in an absorption region", IEEE Trans. Antennas and Propagation, Vol. 26, no.2 pp. 329–332, 1978.

Peled, A. and Liu, B., "Digital signal processing. Theory, design and implementation", (John Wiley & Sons, New York, 1976).

Robins, W.P., "Measurement of propagation parameters in the 20/30 GHz bands", in: Advanced Satellite Communication Systems Using the 20–30 GHz Bands. Proc. Symp. Genoa, 14–16 Dec. 1977. Ed. by G. Berretta et al. Paris: European Space Agency, 1978. ESA SP–138. Pp. 227–236.

Sarma, A.D., Silva Mello, L., Siqueira, G.L., Cole, R.S. and Medeiros Filho, F.C., "Theoretical and experimental investigation of millimeter wave phase fluctuations in an absorption region", International Journal of Infrared and Millimeter Waves, Vol. 7, no. 6, pp. 785–793, 1986.

Sarma, A.D. and Cole, R.S., "Influence of water vapour pressure fluctuations on the spectral density of millimeter wave amplitude scintillations in an absorption region", International Journal of Infrared and Millimeter Waves, Vol. 8, no. 8, pp. 851–856, 1987.

Sarma, A.D., "The influence of oxygen absorption on frequencies near 60 GHz : A mini–review", IETE Tech. Rev. (India), Vol. 5, no. 8, pp. 311–317, 1988.

Sarma, A.D., "Computer programs for acquisition and analysis of scintillation events (OPEX)", Internal report of Telecommunications Division, Faculty of Electrical Engineering, Eindhoven University of Technology, 1989.

Sarma, A.D. and Herben, M.H.A.J., "Variable cut–off frequency filter for wide scintillation bandwidth measurements", Archiv für Elektronik und Übertragungstechnik, Vol. 43, pp. 378–381, 1989.

Sarma, A.D. and Herben, M.H.A.J., "A humidity sensor for scintillation measurements", accepted for publication in the International Journal of Electronics, 1990a.

Sarma, A.D. and Herben, M.H.A.J., "Theoretical investigation of differential phase fluctuations between two coherent radio signals", accepted for publication in Archiv für Elektronik und Übertragungstechnik.

Sarma, A.D., Hill, R.J. and Lataitis, R.J., "Effects of rain on millimeter wave amplitude scintillation spectra". To be presented at: Int. Conf. on Millimeter Wave and Microwave, Dehradun, India, March 14–16, 1990. Defence Electronics Applications Laboratory, Raipur Road, Dehradun – 248001, India.

Shanmugam, K.S., "Digital and analog communication systems", (John Wiley & Sons, New York, 1979).

Tatarskii, V.I., "Wave propagation in a turbulent medium", (McGraw–Hill, New York, 1961).

Travis, B., "High–resolution D/A and A/D converters advance in crucial specifications", EDN, Vol. 30, no. 4, pp. 65–90, Feb. 7, 1985.

van Weert, M.J.M., "The influence of frequency and receiver aperture on the scintillation noise power", in: Electromagnetic Noise Interference and Compatibility. Proc. Joint Avionics/Electromagnetic Wave Propagation Panels Symp., Paris, 21–25 Oct. 1974. Neuilly sur Seine: AGARD, 1975. AGARD Conf. Proc. 159, paper 12, 1975.

Vilar, E. and Haddon, J., "Measurement and modelling of scintillation intensity to estimate turbulence parameters in an earth–space path", IEEE Trans. Antennas and Propagation, Vol. 32, no. 4, pp. 340–346, 1984

Eindhoven University of Technology Research Reports
Faculty of Electrical Engineering

ISSN 0167-9708
Coden: TEUEDE

(205) Butterweck, H.J. and J.H.F. Ritzerfeld, M.J. Werter
FINITE WORDLENGTH EFFECTS IN DIGITAL FILTERS: A review.
EUT Report 88-E-205. 1988. ISBN 90-6144-205-2

(206) Bollen, M.H.J. and G.A.P. Jacobs
EXTENSIVE TESTING OF AN ALGORITHM FOR TRAVELLING-WAVE-BASED DIRECTIONAL DETECTION AND PHASE-SELECTION BY USING TWONFIL AND EMTP.
EUT Report 88-E-206. 1988. ISBN 90-6144-206-0

(207) Schuurman, W. and M.P.H. Weenink
STABILITY OF A TAYLOR-RELAXED CYLINDRICAL PLASMA SEPARATED FROM THE WALL BY A VACUUM LAYER.
EUT Report 88-E-207. 1988. ISBN 90-6144-207-9

(208) Lucassen, F.H.R. and H.H. van de Ven
A NOTATION CONVENTION IN RIGID ROBOT MODELLING.
EUT Report 88-E-208. 1988. ISBN 90-6144-208-7

(209) Jóźwiak, L.
MINIMAL REALIZATION OF SEQUENTIAL MACHINES: The method of maximal adjacencies.
EUT Report 88-E-209. 1988. ISBN 90-6144-209-5

(210) Lucassen, F.H.R. and H.H. van de Ven
OPTIMAL BODY FIXED COORDINATE SYSTEMS IN NEWTON/EULER MODELLING.
EUT Report 88-E-210. 1988. ISBN 90-6144-210-9

(211) Boom, A.J.J. van den
H_∞-CONTROL: An exploratory study.
EUT Report 88-E-211. 1988. ISBN 90-6144-211-7

(212) Zhu Yu-Cai
ON THE ROBUST STABILITY OF MIMO LINEAR FEEDBACK SYSTEMS.
EUT Report 88-E-212. 1988. ISBN 90-6144-212-5

(213) Zhu Yu-Cai, M.H. Driessen, A.A.H. Damen and P. Eykhoff
A NEW SCHEME FOR IDENTIFICATION AND CONTROL.
EUT Report 88-E-213. 1988. ISBN 90-6144-213-3

(214) Bollen, M.H.J. and G.A.P. Jacobs
IMPLEMENTATION OF AN ALGORITHM FOR TRAVELLING-WAVE-BASED DIRECTIONAL DETECTION.
EUT Report 89-E-214. 1989. ISBN 90-6144-214-1

(215) Hoeijmakers, M.J. en J.M. Vleeshouwers
EEN MODEL VAN DE SYNCHRONE MACHINE MET GELIJKRICHTER, GESCHIKT VOOR REGELDOELEINDEN.
EUT Report 89-E-215. 1989. ISBN 90-6144-215-X

(216) Pineda de Gyvez, J.
LASER: A LAyout Sensitivity ExploreR. Report and user's manual.
EUT Report 89-E-216. 1989. ISBN 90-6144-216-8

(217) Duarte, J.L.
MINAS: An algorithm for systematic state assignment of sequential machines - computational aspects and results.
EUT Report 89-E-217. 1989. ISBN 90-6144-217-6

(218) Kamp, M.M.J.L. van de
SOFTWARE SET-UP FOR DATA PROCESSING OF DEPOLARIZATION DUE TO RAIN AND ICE CRYSTALS IN THE OLYMPUS PROJECT.
EUT Report 89-E-218. 1989. ISBN 90-6144-218-4

(219) Koster, G.J.P. and L. Stok
FROM NETWORK TO ARTWORK: Automatic schematic diagram generation.
EUT Report 89-E-219. 1989. ISBN 90-6144-219-2

(220) Willems, F.M.J.
CONVERSES FOR WRITE-UNIDIRECTIONAL MEMORIES.
EUT Report 89-E-220. 1989. ISBN 90-6144-220-6

(221) Kalasek, V.K.I. and W.M.C. van den Heuvel
L-SWITCH: A PC-program for computing transient voltages and currents during switching off three-phase inductances.
EUT Report 89-E-221. 1989. ISBN 90-6144-221-4

Eindhoven University of Technology Research Reports
Faculty of Electrical Engineering

ISSN 0167-9708
Coden: TEUEDF

(222) Józwiak, L.
THE FULL-DECOMPOSITION OF SEQUENTIAL MACHINES WITH THE SEPARATE REALIZATION OF THE NEXT-STATE AND OUTPUT FUNCTIONS.
EUT Report 89-E-222. 1989. ISBN 90-6144-222-2

(223) Józwiak, L.
THE BIT FULL-DECOMPOSITION OF SEQUENTIAL MACHINES.
EUT Report 89-E-223. 1989. ISBN 90-6144-223-0

(224) Book of abstracts of the first Benelux-Japan Workshop on Information and Communication Theory, Eindhoven, The Netherlands, 3-5 September 1989.
Ed. by Han Vinck.
EUT Report 89-E-224. 1989. ISBN 90-6144-224-9

(225) Hoeijmakers, M.J.
A POSSIBILITY TO INCORPORATE SATURATION IN THE SIMPLE, GLOBAL MODEL OF A SYNCHRONOUS MACHINE WITH RECTIFIER.
EUT Report 89-E-225. 1989. ISBN 90-6144-225-7

(226) Dahiya, R.P. and E.M. van Veldhuizen, W.R. Rutgers, L.H.Th. Rietjens
EXPERIMENTS ON INITIAL BEHAVIOUR OF CORONA GENERATED WITH ELECTRICAL PULSES SUPERIMPOSED ON DC BIAS.
EUT Report 89-E-226. 1989. ISBN 90-6144-226-5

(227) Bastings, R.H.A.
TOWARD THE DEVELOPMENT OF AN INTELLIGENT ALARM SYSTEM IN ANESTHESIA.
EUT Report 89-E-227. 1989. ISBN 90-6144-227-3

(228) Hekker, J.J.
COMPUTER ANIMATED GRAPHICS AS A TEACHING TOOL FOR THE ANESTHESIA MACHINE SIMULATOR.
EUT Report 89-E-228. 1989. ISBN 90-6144-228-1

(229) Oostrom, J.H.M. van
INTELLIGENT ALARMS IN ANESTHESIA: An implementation.
EUT Report 89-E-229. 1989. ISBN 90-6144-229-X

(230) Winter, M.R.M.
DESIGN OF A UNIVERSAL PROTOCOL SUBSYSTEM ARCHITECTURE: Specification of functions and services.
EUT Report 89-E-230. 1989. ISBN 90-6144-230-3

(231) Schemmann, M.F.C. and H.C. Heyker, J.J.M. Kwaspen, Fr.G. van de Roer
MOUNTING AND DC TO 18 GHz CHARACTERISATION OF DOUBLE BARRIER RESONANT TUNNELING DEVICES.
EUT Report 89-E-231. 1989. ISBN 90-6144-231-1

(232) Sarma, A.D. and M.H.A.J. Herben
DATA ACQUISITION AND SIGNAL PROCESSING/ANALYSIS OF SCINTILLATION EVENTS FOR THE OLYMPUS PROPAGATION EXPERIMENT.
EUT Report 89-E-232. 1989. ISBN 90-6144-232-X